Rac-GAP α-Chimerin Regulates Motor-Circuit Formation as a Key Mediator of EphrinB3/EphA4 Forward Signaling

Takuji Iwasato,[1,*] Hironori Katoh,[2] Hiroshi Nishimaru,[3] Yukio Ishikawa,[2] Haruhisa Inoue,[4] Yoshikazu M. Saito,[1] Reiko Ando,[1] Mizuho Iwama,[1] Ryosuke Takahashi,[4] Manabu Negishi,[2] and Shigeyoshi Itohara[1]

[1]Laboratory for Behavioral Genetics, RIKEN Brain Science Institute (BSI), 2-1 Hirosawa Wako-shi, Saitama 351-0198, Japan
[2]Laboratory of Molecular Neurobiology, Graduate School of Biostudies, Kyoto University, Yoshidakonoe-cho, Sakyo-ku, Kyoto 606-8501, Japan
[3]Neuroscience Research Institute, National Institute of Advanced Industrial Science and Technology (AIST), 1-1-1 Higashi, Tsukuba, Ibaraki 305-8566, Japan
[4]Department of Neurology, Kyoto University Graduate School of Medicine, 54 Kawahara-cho, Shogoin, Sakyo-ku, Kyoto 606-8507, Japan
*Correspondence: iwasato@brain.riken.jp
DOI 10.1016/j.cell.2007.07.022

SUMMARY

The ephrin/Eph system plays a central role in neuronal circuit formation; however, its downstream effectors are poorly understood. Here we show that α-chimerin Rac GTPase-activating protein mediates ephrinB3/EphA4 forward signaling. We discovered a spontaneous mouse mutation, miffy (mfy), which results in a rabbit-like hopping gait, impaired corticospinal axon guidance, and abnormal spinal central pattern generators. Using positional cloning, transgene rescue, and gene targeting, we demonstrated that loss of α-chimerin leads to mfy phenotypes similar to those of EphA4^{−/−} and ephrinB3^{−/−} mice. α-chimerin interacts with EphA4 and, in response to ephrinB3/EphA4 signaling, inactivates Rac, which is a positive regulator of process outgrowth. Moreover, downregulation of α-chimerin suppresses ephrinB3-induced growth cone collapse in cultured neurons. Our findings indicate that ephrinB3/EphA4 signaling prevents growth cone extension in motor circuit formation via α-chimerin-induced inactivation of Rac. They also highlight the role of a Rho family GTPase-activating protein as a key mediator of ephrin/Eph signaling.

INTRODUCTION

Ephrins are cell-surface-bound ligands for Eph receptors, which comprise the largest family of receptor tyrosine kinases (Eph Nomenclature Committee, 1997). The ephrin/Eph interaction induces bidirectional signaling: ephrin → Eph forward and Eph → ephrin reverse (Noren and Pasquale, 2004; Palmer and Klein, 2003). Ephrin/Eph signaling, which functions in short-range cell-to-cell communication primarily through repulsive effects, is central to neuronal circuit development (Flanagan and Vanderhaeghen, 1998; Palmer and Klein, 2003; Pasquale, 2005).

Downstream signaling has been studied mostly through in vitro cell culture experiments. Particularly important players in both forward and reverse signaling are the Rho-family GTPases (Rho-GTPases), such as RhoA, Rac, and Cdc42, which are the key regulators of actin dynamics (Etienne-Manneville and Hall, 2002; Luo, 2000; Noren and Pasquale, 2004; Wahl et al., 2000). Rho-GTPases are directly activated by Rho-guanine nucleotide-exchange factors (Rho-GEFs) and are inactivated by Rho-GTPase-activating proteins (Rho-GAPs). Accumulating evidence suggests that ephrin/Eph regulates Rho-GTPases through Rho-GEFs (Cowan et al., 2005; Irie and Yamaguchi, 2002; Murai and Pasquale, 2005; Ogita et al., 2003; Penzes et al., 2003; Shamah et al., 2001; Tanaka et al., 2004).

Among the numerous Rho-GEFs involved in ephrin/Eph signaling, ephexin1 is the best characterized. EphA receptors are thought to regulate growth cone dynamics through ephexin1 in axon guidance (Sahin et al., 2005; Shamah et al., 2001). Activation of RhoA induces growth cone retraction and/or collapse, while activated Rac and Cdc42 promote its extension (Etienne-Manneville and Hall, 2002; Luo, 2000). The engagement of Ephs by ephrin leads to activation of the GEF activity of ephexin1 toward RhoA, thereby causing growth cone collapse in vitro (Shamah et al., 2001). However, as ephexin1-knockout (KO) mice are apparently normal (Sahin et al., 2005), the role of ephexin1 remains largely unknown. It is also noteworthy that, compared with the considerable attention given to Rho-GEFs, the possible contribution of Rho-GAPs in actin dynamics controlled by ephrin/Eph signaling has largely been neglected.

The roles of ephrin/Eph signaling in vivo have been studied using mouse reverse genetics. An extremely well-characterized case is ephrinB3 → EphA4 forward signaling. $EphrinB3^{-/-}$ and $EphA4^{-/-}$ mice both display several neural phenotypes, including a rabbit-like hopping gait and impairment of two major motor circuits: the corticospinal tract (CST) and the spinal neuronal circuit controlling locomotion, which is also known as the central pattern generator (CPG). Similar phenotypes are also displayed by $EphA4^{KD/KD}$ and $EphA4^{FF/FF}$ mice, both of which have impaired kinase activity of EphA4, but not by mice expressing a truncated form of ephrinB3 lacking its cytoplasmic domain (Dottori et al., 1998; Kullander et al., 2003, 2001a, 2001b; Yokoyama et al., 2001). Thus, it is apparent that ephrinB3 → EphA4 forward signaling, but not EphA4 → ephrinB3 reverse signaling, is essential for the formation of these motor circuits.

CST axons controlling voluntary movements arise in the motor cortex, cross into the contralateral side of the medulla, and enter the spinal cord (Gianino et al., 1999; Liang et al., 1991). In wild-type (WT) mice, they rarely cross back to the other side in the spinal cord because ephrinB3 is anchored at the midline and generates repulsive signals through EphA4 receptors expressed on the surface of the CST axon membranes. In *ephrinB3* or *EphA4* mutant mice, due to a lack of repulsive ephrinB3/EphA4 forward signaling, many CST axons fail to stop at the midline and recross it (Kullander et al., 2001a; Yokoyama et al., 2001). Spinal CPGs are thought to generate the repetitive sequential stepping of limbs during walking (Grillner and Wallen, 1985). Locomotor-like rhythmic activity, alternating between the left and right sides, can be evoked in the isolated spinal cords of WT mice (Nishimaru and Kudo, 2000), whereas the activity of the two sides is synchronous in the spinal cords of $ephrinB3^{-/-}$ or $EphA4^{-/-}$ mice (Kullander et al., 2003). Aberrant midline crossing of axons from EphA4-expressing CPG interneurons is thought to be responsible for the CPG abnormality in $ephrinB3^{-/-}$ and $EphA4^{-/-}$ mice (Kiehn and Kullander, 2004; Kullander et al., 2003).

The current study provides both in vivo and in vitro evidence that the Rac-specific GAP α-chimerin plays a critical role in the formation of CST and CPGs as an essential downstream component of ephrinB3/EphA4 forward signaling.

RESULTS

A Novel Spontaneous Autosomal Recessive Mutation leading to a Rabbit-like Hopping Gait

We unexpectedly discovered mutant mice with a rabbit-like gait while generating mice homozygous for a ChAT-Cre#23 construct (Inoue et al., 2003). This mutation, which we designated as *miffy* (*mfy*), was autosomal recessive. We initially assumed that *mfy* was caused by gene disruption during transgene integration. However, this was not the case because the *mfy* locus segregated from the transgene, suggesting that the mutation arose spontaneously. *mfy/mfy* mice appeared in crosses at the expected Mendelian frequency and were healthy and fertile. Their bodies were slightly smaller than their littermate controls during the postnatal developmental period. For instance, on postnatal day 10 (P10), the average body weights ± standard error of the mean (SEM) were 4.68 ± 0.17 g, 5.68 ± 0.17 g, and 5.80 ± 0.15 g for the *mfy/mfy* (n = 10), *mfy/+* (n = 12), and *+/+* (n = 5) pups, respectively. However, these differences were not evident in adulthood.

WT and *mfy/+* mice moved with a normal alternate step gait. By contrast, all of the *mfy/mfy* mice (n > 100) tended to move their left and right hind limbs synchronously, resulting in a rabbit-like hopping gait (Figure 1A). The mean ± SEM proportion of left-right synchronized gaits among 40 randomly selected gaits was 0 for *mfy/+* (n = 13) and 98.42% ± 0.61% for *mfy/mfy* (n = 19) mice (p < 0.0001, unpaired t test). The gross morphology of the *mfy/mfy* mouse brain was indistinguishable from that of its littermate controls (WT and *mfy/+* mice; Figures S1A and S1B). By contrast, a morphological analysis of cross-sections of the spinal cord of *mfy/mfy* mice revealed that the white matter in the dorsal funiculus was reduced, most prominently at the lumbar levels (Figure S1C).

Aberrant Recrossing of CST Axons at the Midline of the Spinal Cord in *mfy/mfy* Mice

The CST axons control voluntary movements through direct or indirect contact with spinal motor neurons (Liang et al., 1991). To visualize these axons, we injected anterograde tracer into the left motor cortex and stained the projections of the CST axons in the medulla and spinal cord. CST axons arising in the left motor cortex crossed to the right side of the medulla in both *mfy/mfy* and control mice (Figure S1D). However, in the spinal cord of control mice (n = 11), CST axons projected only into the contralateral (right) gray matter and barely recrossed the midline into the ipsilateral gray matter, whereas we observed aberrant midline recrossing of these axons in all of the preparations of *mfy/mfy* mouse spinal cords examined (n = 7; Figures 1B and 1C).

To confirm the anterograde tracing results, we injected a retrograde tracer unilaterally into the lumber spinal cord (Figure 1D). In WT mice, most of the retrograde-labeled CST neurons were located in layer V of the contralateral motor cortex (Figure 1E). However, in *mfy/mfy* mice, the ipsilateral cortex also contained many labeled neurons (Figure 1F). Cell-count analyses of the motor cortex revealed that the ipsilateral cortex of WT (n = 4) and *mfy/mfy* (n = 7) mice contained 2.02% ± 0.92% and 34.26% ± 5.22% times as many labeled cells as the contralateral cortex, respectively, which was statistically significant (p < 0.002; Figure 1G).

Abnormal CPGs in the Spinal Cord of *mfy/mfy* Mice

To examine the locomotor CPGs underlying limb movements during walking, we isolated the spinal cords from newborn (P1–P3) *mfy/mfy* and control (*mfy/+* and WT) mice and induced locomotor-like activity by applying

A control   *mfy/mfy*   **B**

control   *mfy/mfy*

ipsilateral   contralateral   ipsilateral   contralateral

C

D   control   *mfy/mfy*

control   *mfy/mfy*

E contralateral
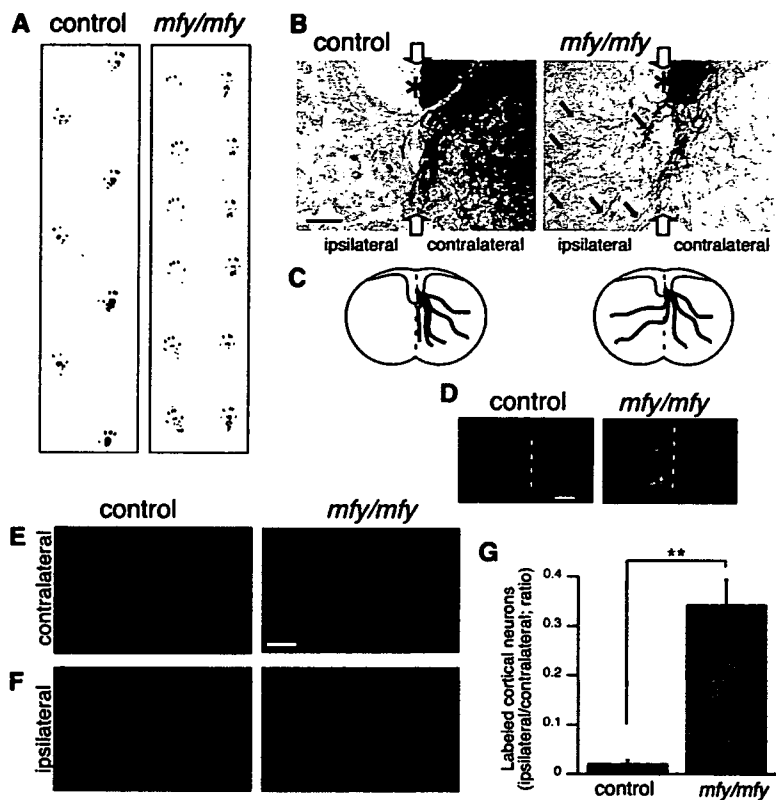
F ipsilateral

G

control   *mfy/mfy*

Figure 1. Abnormal Walking and CST Axon Guidance in the Novel Spontaneous Mutant *mfy*

(A) Representative hind-limb footprint patterns. Hind limbs were painted with black ink, and the mice were placed on white paper.

(B) Anterograde tracings of CST axons by biotinylated dextran amine (BDA) and sectioning at cervical levels of the spinal cord. CST axons positioned within the dorsal funiculus (asterisk) on the contralateral side to the tracer injection projected into the spinal gray matter in both control and *mfy/mfy* mice; however, in the *mfy/mfy* mice only, many of the CST axons (blue arrows) recrossed the midline (white arrows).

(C) Schematics of CST axons (red) in the spinal cord.

(D) A fluorescent retrograde tracer cholera toxin B (CTB) was unilaterally injected into the lumbar spinal cord.

(E and F) In the motor cortex layer V of control (WT) mice, most of the labeled neurons were located in the contralateral side (E). In *mfy/mfy* mice, the ipsilateral side also contained many labeled neurons (F).

(G) The ipsilateral/contralateral ratio of numbers of labeled cortical neurons in *mfy/mfy* mice (n = 7) was significantly higher than that of control mice (n = 4). Data are represented as the mean ± SEM: Student's t test, $p < 0.002$. Scale bars: 100 μm.

N-methyl-D-aspartate (NMDA) and serotonin. The ventral root (VR) activity of lumber 2 (L2) represents flexor muscle activity during locomotion, while that of L5 represents extensor activity (Whelan et al., 2000). In control mice, we observed alternation between the left and right L2s (Figures 2A–2C), whereas the cords of *mfy/mfy* mice displayed a synchronous rhythm of the left and right L2s (Figures 2A–2C). The rhythmic activity of the flexors (L2) and extensors (L5) of each limb alternated in both control and *mfy/mfy* mice spinal cords (Figures 2A–2C). We injected a tracer unilaterally into the ventral side of the spinal cords of P4 *mfy/mfy* and control pups, and we found that more neuronal fibers, presumably derived from ipsilateral-projecting interneurons, crossed the midline in the *mfy/mfy* spinal cords than in the control spinal cords (Figure 2D; for quantitative analyses, see Figures S2A and S2B).

The *mfy* Locus Encodes the Rac-Specific GAP α-Chimerin

To locate the *mfy* locus, we employed microsatellites and single-nucleotide polymorphisms (SNPs) that distinguish between the alleles of two inbred mouse strains, DBA/2 (DBA) and C57BL/6 (B6). The *mfy* mutant was identified and maintained in a pure B6 genetic background. We therefore crossed *mfy/mfy* mice with WT DBA mice and obtained *mfy/+* mice in a B6/DBA F_1 genetic background. By backcrossing these F_1 mice to *mfy/mfy* mice and genotyping the DNA of the 299 backcross progeny, we mapped the *mfy* locus to the region between SNPs

rs13476571 and *rs13459064* on chromosome 2 (Figure S3).

In total, 30 genes are known within this 3.27 Mb interval (Table S1). Among these, 10 genes could be excluded because their KO mouse lines have been previously reported to survive to adulthood, and they do not appear to have hopping gaits (for references, see Table S1). We compared the sizes and transcript levels of the remaining 20 genes in the brains of WT and *mfy/mfy* mice at P5 using the reverse transcription-polymerase chain reaction (RT-PCR) with primer sets amplifying the complementary DNA (cDNA) between the 5′ and 3′ untranslated regions (UTRs) and found that the transcripts of only one gene, the α-chimerin (*α-Chn*) gene, differed in size (Figures 3A and 3B; Table S1). α-chimerin is a Rho-GAP that is specific for the positive regulator of actin polymerization, Rac (Diekmann et al., 1991; Hall et al., 1990, 1993). Recent reports using overexpression and/or small-interfering RNA (siRNA)-mediated knockdown in cultured neurons and/or tissue slices suggest that α-chimerin is involved in regulating dendritic morphology and spine density (Buttery et al., 2006; Van de Ven et al., 2005) as well as semaphorin3A-induced growth cone collapse (Brown et al., 2004). However, the role of α-chimerin in living animals has not yet been defined.

α-Chn has two splice isoforms: α1 and α2 (Hall et al., 1990, 1993). A comparison of the sequences of the *α1-Chn* and *α2-Chn* cDNAs of WT and *mfy/mfy* mice revealed that exon 9 (174 base pairs [bp]) was deleted in the
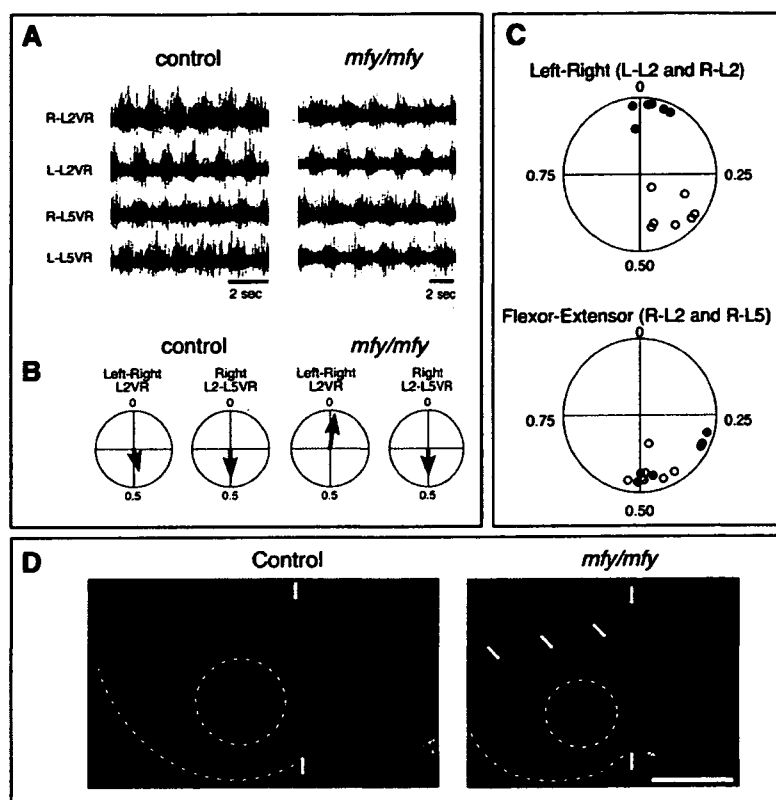
Figure 2. Synchronous Left-Right VR Activity in the Lumbar Spinal Cord of mfy/mfy Mice

(A) Locomotor-like motor activity recorded after bath-application of NMDA and serotonin to isolated spinal cords of control and mfy/mfy mice. VR activity of the second (L2) and fifth (L5) lumbar segments on the left (L-) and right (R-) sides was recorded using glass-suction electrodes.

(B) Circular phase diagrams for the locomotor-like rhythmic activity of the control and mfy/mfy mice shown in (A). Phase relationships between L-L2VR and R-L2VR (left panel) and flexor (R-L2VR) and extensor (R-L5VR) on one side of the lumbar cord (right panel) are indicated in each diagram derived from 30 locomotor cycles. Locomotor cycles in which the two VR activities are in complete alternation have phase values of 0.5. Those that are completely synchronous have phase values of 0 or 1. The mean phase and the r value, which describes the concentration of phase values around the mean, are shown by the direction and magnitude, respectively, of the vector originating from the center of the circle.

(C) Summary plots of seven control (open circles) and six mfy/mfy (filled circles) mice at P1–P3.

(D) Transverse spinal cord sections (100 μm thick) at the L2 level after unilateral application of DiI on the ventral side of L4. More neuronal fibers (yellow arrows), which are likely to be derived from ipsilateral-projecting interneurons, crossed the midline (white arrows) to the contralateral (left) side in mfy/mfy spinal cords than in control spinal cords. The cell bodies of descending commissural interneurons, shown by dotted circles, were indistinguishable. Scale bar: 500 μm.

$\alpha 1$-Chn^{mfy} and $\alpha 2$-Chn^{mfy} transcripts (Figure 3A). Exon 9 encodes 58 amino acids, three of which (EIE) are known to be essential for the GAP activity of α-chimerin that inactivates Rac (Ahmed et al., 1994); $\alpha 2$-chimerin^{mfy} was indeed found to lack Rac-GAP activity in vitro (Figure S4). In addition to the $\alpha 1$ and $\alpha 2$ isoforms, we found transcripts of a putative novel isoform that we termed $\alpha 3$ (Figures 3A and 3B). In the $\alpha 3$-Chn^{mfy} transcript, four nucleotides (GATG) of exon 9, including the putative initiation codon, were replaced with retroposon sequences, and intron 9 failed to be excised (Figure 3A). The cloning and sequencing of the genomic DNA of the mfy allele revealed an insertion of a retroposon into exon 9, which appeared to impair both the donor and the acceptor splicing functions (Figure 3A). Quantitative RT-PCR demonstrated strong $\alpha 2$-Chn expression, weak $\alpha 1$-Chn expression, and little $\alpha 3$-Chn expression in the motor cortex and spinal cord of P4 WT mice (Figure 3C). We therefore focused on the $\alpha 2$ isoform in subsequent studies. We raised an $\alpha 2$-chimerin-specific polyclonal antibody and confirmed by western blot analysis that the $\alpha 2$-chimerin^{WT} protein could not be detected in the mfy/mfy brain (Figure 3D). Further-

more, even the $\alpha 2$-chimerin^{mfy} protein was barely detected in the mfy/mfy brain and spinal cord (Figures 3D and 3E), suggesting that endogenous $\alpha 2$-chimerin^{mfy} is much less stable in neurons than $\alpha 2$-chimerin^{mfy} overexpressed in cultured cells (Figure S4B).

Improved Locomotor Behavior of mfy/mfy Mice Expressing Transgenic α-Chn

To confirm that α-Chn was the mfy gene, we tested whether transgenic (Tg) expression of α-Chn rescued the mfy phenotype. We modified a bacterial artificial chromosome (BAC) clone that covered the 49 kb upstream region and exons 1–7 of α-Chn using Red/ET homologous recombination and flp/FRT recombination in order to make a BAC α-Chn construct in which exon 7 was followed by a cDNA encoding exons 8–13 and a poly(A) signal (Figure 4A). We then generated two lines (#539 and #883) of BAC Tg mice by microinjecting the construct into pronuclei and mated them with mfy/mfy mice to obtain Tg mice in the mfy/mfy background (Figure 4B). There were no improvements in the gaits of the Tg#539:mfy/mfy mice (see Figure S5 legend), consistent with no detectable
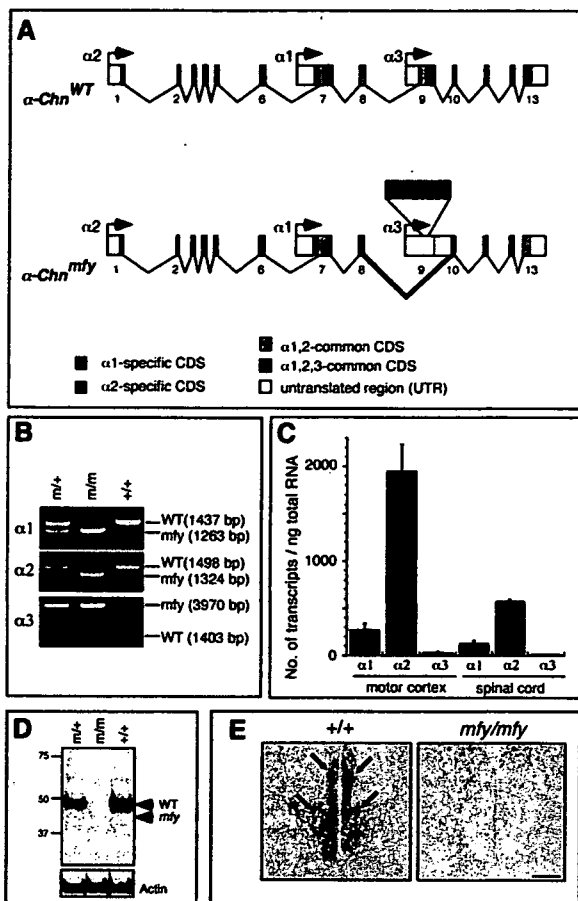
Figure 3. The mfy Locus Encodes α-Chimerin Rac-GAP

(A) Schematic exon-intron structures of α1-Chn, α2-Chn, and α3-Chn splicing variants for the WT (α-Chn^WT) and mfy (α-Chn^mfy) alleles. Retroposon (Tn) insertion into exon 9 in the mfy mutant resulted in deletion (red lines) of exon 9 (174 bp) in the α1 and α2 transcripts, and deletion of four nucleotides (including the putative initiation codon) and failure of intron 9 splicing in the α3 transcript. CDS: coding sequences.

(B) RT–PCR products from between the 5′ UTR and the 3′ UTR of the α1-Chn, α2-Chn, and α3-Chn splicing isoforms in cDNAs derived from WT (+/+), mfy/+ (m/+), and mfy/mfy (m/m) brains at P5. PCR products from the WT and mutant (mfy) α1-Chn, α2-Chn, and α3-Chn isoforms were purified and cloned, and their nucleotide sequences were determined.

(C) α2-Chn predominates in the developing motor cortex and spinal cord. Real-time quantitative RT-PCR of α1-Chn, α2-Chn, and α3-Chn in the motor cortex and spinal cord of WT mice at P4. All data are presented as the mean ± SEM (n = 3 mice).

(D) Western blot using an α2-chimerin-specific antibody revealed that α2-chimerin^WT protein (WT) was absent from mfy/mfy mice. Unexpectedly the mutant protein (mfy) was barely detectable in mfy/+ and mfy/mfy mice. Total lysates from P10 of the mouse telencephalon were used.

(E) Immunohistochemistry using α2-chimerin-specific antibody revealed strong expression of α2-chimerin in the CST (arrows) of the dorsal funiculus (dotted line) of the WT spinal cord, suggesting that α2-chimerin functions in developing CST axons. α-chimerin was not detectable in mfy/mfy spinal cords. Scale bar: 50 μm.

α-chimerin expression in these mice (Figures S5A and S5B). By contrast, considerable improvement was observed in the gaits of the Tg#883:mfy/mfy mice (Figure 4C). The average ± SEM proportion of left-right synchronized gaits in 40 randomly selected gaits of Tg#883:mfy/mfy mice (n = 13) was 53.65% ± 6.56%, which was substantially less than in their littermate mfy/mfy mice (n = 6, 99.58% ± 0.42%; p < 0.0001, unpaired t test). α-chimerin protein was expressed at low levels in Tg#883:mfy/mfy mice (Figures S5A–S5C), which was consistent with the moderate rescue of gait observed in these mice. These results strongly suggest that α-Chn is the causal gene of the mfy mutation.

Generation and Characterization of α-Chn KO Mice

To further confirm that the mfy gene encoded α-Chn, we deleted exons 9 and 10 from the allele by a gene-targeting technique in embryonic stem (ES) cells and Cre/loxP recombination in the mouse germline and generated mice homozygous for the targeted allele (α-Chn KO mice; Figures 4D and S5D). These mice had a hopping gait similar to that of mfy/mfy mice (Figure 4E). They also demonstrated aberrant midline recrossing of CST axons (Figure 4F), aberrant midline crossing of spinal local circuit neurons (Figure S2C), and shorter ventral extension of the dorsal funiculus in the spinal cord (data not shown). Furthermore, they showed abnormal spinal CPGs (Figures 4G and S6). All of these phenotypes were similar to those of mfy/mfy mice. Thus, we concluded that the mfy phenotypes were caused by α-Chn disruption.

Localization of α-Chimerin Proteins in CST

The phenotypes of mfy/mfy and α-Chn KO mice (hopping gait, Figures 1A and 4E), abnormal spinal-cord morphology (Figure S1C), abnormal CPGs (Figures 2C and 4G), aberrant midline crossing by CPG axons (Figures 2D and S2), and aberrant midline recrossing by CST axons (Figures 1B and 4F) appeared to be identical to those reported for ephrinB3^−/− and EphA4^−/− mice (Dottori et al., 1998; Kullander et al., 2003, 2001a; Yokoyama et al., 2001) and for EphA4^FF/FF and EphA4^KD/KD mice expressing a mutant EphA4 lacking kinase activity (Kullander et al., 2001b). Nevertheless, the anterior commissure, the formation of which is known to be dependent on EphA4 reverse signaling (Kullander et al., 2001b), appeared normal in mfy/mfy mice (Figure S1B). Hence, it seemed likely that the mfy phenotype was caused by impairment of ephrinB3/EphA4 forward signaling.

Using immunohistochemistry, we found that α2-chimerin colocalized with EphA4 in the developing CST (Figures S7A and S7C). In α-Chn KO CST, α2-chimerin was not detected, but the levels of EphA4 expression appeared to be unaltered (Figures S7B and S7D). We also found that the α2-chimerin protein was present in the growth cones of cultured neurons derived from the anterior dorsomedial to dorsal neocortex (motor cortex; Figure S8C). These results suggest that α-chimerin functions
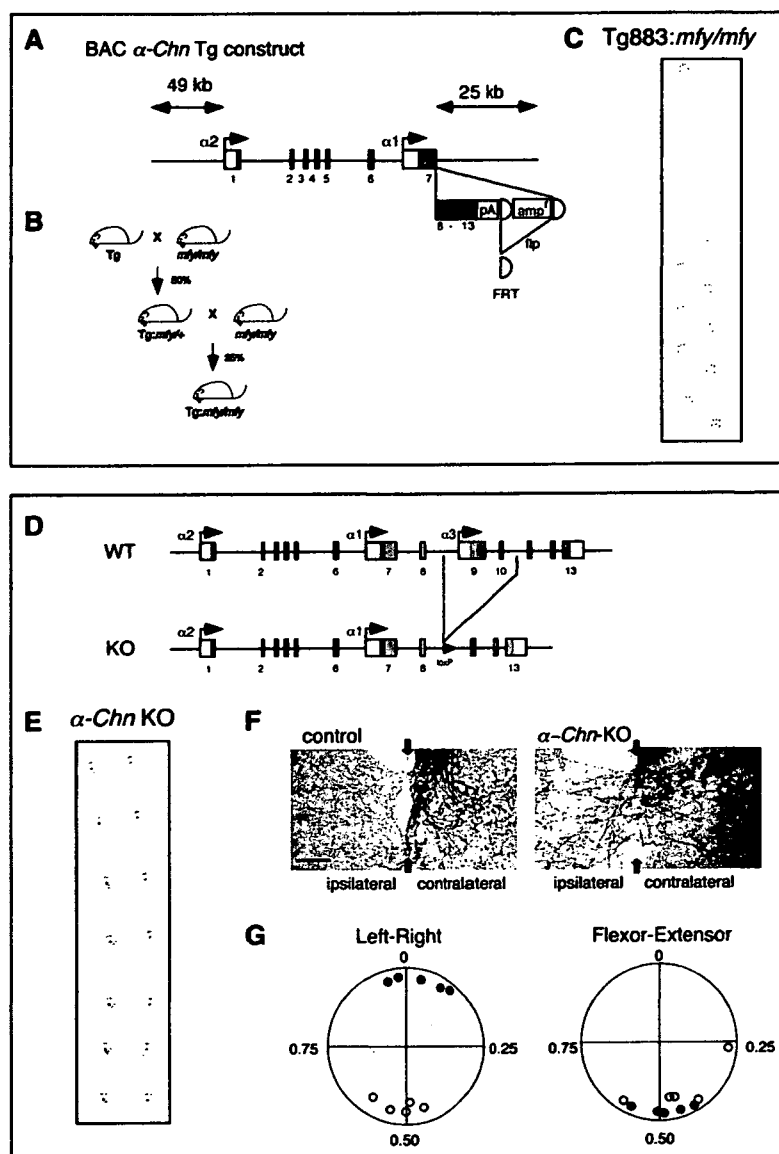
Figure 4. Disruption of α-Chn Is Responsible for the mfy Phenotypes

(A) Schematic of the BAC Tg construct. A cDNA fragment containing exons 8–13, a poly(A) signal, and an amp^r selection marker flanked by two FRT sites was inserted immediately after exon 7 of a BAC clone covering exons 1–7 of α-Chn, using Red/ET homologous recombination in bacteria. Amp^r was removed from the BAC construct by expressing flp recombinase in the bacterial clone.

(B) Tg mouse lines were generated by injecting the linearized construct into fertilized mouse eggs. Two lines of Tg mice were crossed with mfy/mfy mice to yield Tg;mfy/+ mice. These were then crossed with mfy/mfy mice to obtain Tg mice in a mfy/mfy background.

(C) Improved walking of Tg#883;mfy/mfy mice. All Tg#883;mfy/mfy mice showed a marked improvement in the control of walking.

(D) Schematic of the KO allele, in which exons 9 and 10 were deleted by homologous recombination in ES cells, and Cre/loxP recombination in the mouse germline.

(E) Representative hind-limb footprint patterns of α-Chn KO mice showing a hopping gait similar to that of mfy/mfy mice.

(F) Anterograde tracing of CST axons and sectioning at cervical levels of the spinal cord. CST axons of α-Chn KO mice aberrantly recrossed the spinal cord midline, as seen in mfy/mfy mice. Scale bar: 100 μm.

(G) Circular phase diagrams for the locomotor-like activity of five control (open circles) and five α-Chn KO (filled circles) mice at P1–P3. Left-right VR activity in the lumber spinal cord of α-Chn KO mice was synchronous as that of mfy/mfy mice.

as a downstream mediator of ephrinB3/EphA4 forward signaling in developing CST axons.

Interaction between α-Chimerin and EphA4

To test whether α-chimerin interacts with EphA4, we cotransfected 293T cells with EphA4 and α-Chn-expression constructs and immunoprecipitated EphA4 from cell lysates with Fc region-fused ephrinA1. Both α1-chimerin and α2-chimerin were precipitated with EphA4^WT and kinase-dead EphA4^FF (Figure 5A), and α2-chimerin^mfy was also precipitated with EphA4 (Figure S9). These results suggest that α-chimerin interacts with EphA4 in vitro and that this interaction does not require the kinase activity of EphA4 or the GAP activity of α-chimerin. To identify the region of α-chimerin responsible for interacting with EphA4, we performed an in vitro glutathione S-transferase (GST) fusion protein pull-down assay. EphA4 was co-

precipitated with full-length α2-chimerin and the α1- and α2-common carboxy (C) terminus, but not with the α2-specific amino (N)-terminus (Figure 5B). These results show that EphA4 associates with α1-chimerin and α2-chimerin at their C termini.

Next we examined whether α-chimerin interacts with EphA4 in neurons, and, if so, whether ligand stimulation enhances the interaction. EphA4 was coprecipitated with α2-chimerin without ligand stimulation, and the amount of EphA4 precipitated with α2-chimerin was not increased following stimulation with clustered ephrinB3 (Figure 5C). These results indicate that α-chimerin associates with EphA4 in neurons and that this interaction is independent of ephrinB3-stimulation. Finally, we prepared lysates from the developing motor cortex of WT mice and immunoprecipitated them with anti-α2-chimerin antibody. EphA4 was again precipitated with α2-chimerin (Figure 5D).
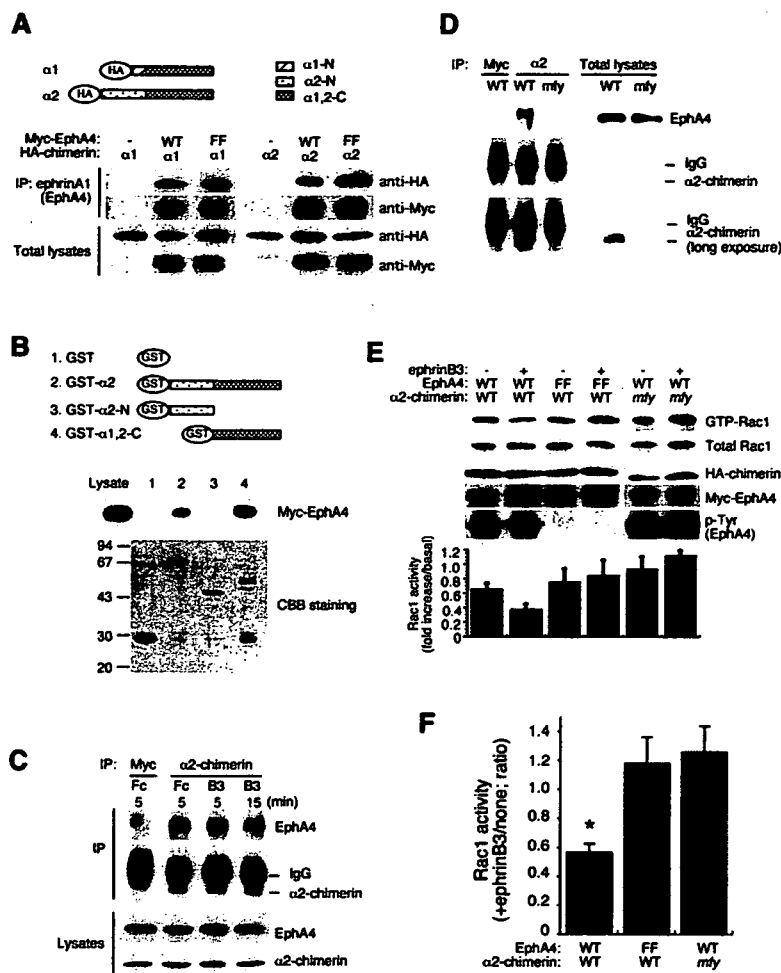
A

α1 (HA)━━━━━
α2 (HA)━━━━━━

▨ α1-N
▥ α2-N
▦ α1,2-C

Myc-EphA4: - WT FF - WT FF
HA-chimerin: α1 α1 α1 α2 α2 α2

IP: ephrinA1 (EphA4) — anti-HA
— anti-Myc

Total lysates — anti-HA
— anti-Myc

B

1. GST (GST)
2. GST-α2 (GST)━━━━━━
3. GST-α2-N (GST)━━
4. GST-α1,2-C (GST)━━━━━━

Lysate 1 2 3 4

● ● ● Myc-EphA4

94 —
67 —
43 — CBB staining
30 —
20 —

C

IP: Myc α2-chimerin
Fc Fc B3 B3
5 5 5 15 (min)

IP
EphA4
— IgG
— α2-chimerin

Lysates
EphA4
α2-chimerin

D

IP: Myc α2 Total lysates
WT WT mfy WT mfy

— EphA4

— IgG
— α2-chimerin

— IgG
— α2-chimerin (long exposure)

E

ephrinB3: - + - + - +
EphA4: WT WT FF FF WT WT
α2-chimerin: WT WT WT WT mfy mfy

GTP-Rac1
Total Rac1
HA-chimerin
Myc-EphA4
p-Tyr (EphA4)

Rac1 activity (fold increase/basal)
1.2
1.0
0.8
0.6
0.4
0.2
0

F

Rac1 activity (+ephrinB3/none; ratio)
1.4
1.2
1.0
0.8
0.6
0.4
0.2
0

EphA4: WT FF WT
α2-chimerin: WT WT mfy

Figure 5. α-Chimerin Interacts with EphA4 and Regulates Rac1 Activity in Response to EphrinB3 → EphA4 Forward Signaling

(A) EphA4 bound to α1-chimerin and α2-chimerin in vitro. Kinase-dead EphA4^{FF} also bound to both isoforms. 293T cells were transfected with the indicated expression plasmids. Total lysates were precipitated with Fc region-fused ephrinA1 and immunoblotted with anti-HA and anti-Myc antibodies to detect α-chimerin and EphA4, respectively. Total lysates were also blotted with anti-HA and anti-Myc antibodies.

(B) EphA4 interacted with the α-chimerin C terminus that is common to both α1 and α2 isoforms. For pulldown assays, HEK293T cells transfected with Myc-tagged EphA4 were lysed, and supernatants were incubated with GST-fusion proteins of α2-chimerin and its deletion mutants, followed by incubation with glutathione-Sepharose beads. Bound proteins were analyzed by SDS-PAGE and immunoblotting with anti-Myc antibody. The lower panel shows Coomassie brilliant blue (CBB) staining of GST-fusion proteins used in this experiment.

(C) Endogenous α-chimerin and EphA4 interacted in neurons, and ephrinB3-stimulation did not enhance this interaction. Cultured cortical neurons from E18.5 rats were stimulated with preclustered ephrinB3-Fc or control Fc for 5 or 15 min. Bound and total proteins were analyzed by immunoblotting with antibodies against EphA4 and α2-chimerin.

(D) Endogenous α-chimerin and EphA4 interacted in the mouse brain. Lysates from a P3 mouse cortex were immunoprecipitated with anti-α2-chimerin antibody or anti-Myc anti-body (a negative control). The mfy/mfy cortex was used as a second negative control. Bound and total proteins were analyzed by immunoblotting with antibodies against EphA4 and α2-chimerin.

(E) COS-7 cells transfected with the indicated plasmids were stimulated with preclustered ephrinB3-Fc (+) or Fc (−) for 10 min. GTP-bound Rac1 was identified by SDS-PAGE and immunoblotting, and its levels were measured and normalized to the corresponding total Rac1 levels. The means and SEMs of Rac1 activity (fold increase/basal) are shown at the bottom.

(F) Statistical analysis of the data shown in (E). EphrinB3-stimulation inactivated Rac1 in cells expressing both EphA4^{WT} and α-chimerin^{WT}, but not in cells expressing EphA4^{FF} and α-chimerin^{WT} or EphA4^{WT} and α-chimerin^{mfy}. n = 4 (EphA4^{WT} + α2-chimerin^{WT}), 5 (EphA4^{FF} + α2-chimerin^{WT}), or 3 (EphA4^{WT} + α2-chimerin^{mfy}). All data are presented as the mean ± SEM. ($^*p < 0.05$, ANOVA/Tukey HSD).

α-Chimerin Inactivates Rac in Response to EphrinB3/EphA4 Forward Signaling In Vitro

No previous reports have suggested the involvement of α-chimerin in ephrin/Eph signaling. To determine whether α-chimerin regulates Rac activity in response to ephrinB3/EphA4 forward signaling, we transfected COS-7 cells with EphA4 (EphA4^{WT} or kinase-dead EphA4^{FF}) and α2-chimerin (α-chimerin^{WT} or α-chimerin^{mfy}) and measured the Rac activity in the presence or absence of ephrinB3 stimulation (Figure 5E). We found that ephrinB3 stimulation inactivated Rac in cells expressing EphA4^{WT} and α-chimerin^{WT}, but not in cells expressing either EphA4^{FF} and α-chimerin^{WT} or EphA4^{WT} and α-chimerin^{mfy} (Figure 5F). These results indicate that both EphA4 kinase activity and functional α-chimerin are required for ephrinB3 stimulation to inactivate Rac. It is noteworthy that the EphA4

proteins overexpressed in COS cells were phosphorylated, and, therefore, kinase active, but were unable to fully activate α-chimerin in the absence of ephrinB3 stimulation (Figure 5E). These results suggest that EphA4 kinase activity alone is not sufficient for activating the Rac-GAP of α-chimerin (see Discussion).

Downregulation of α-Chimerin Suppresses EphrinB3-Induced Growth Cone Collapse in Cultured Cortical Neurons

EphrinB3/EphA4 forward signaling induces growth cone collapse in cultured neurons derived from the motor cortex (Egea et al., 2005; Kullander et al., 2001a). To determine whether α-chimerin regulates growth cone dynamics downstream of ephrinB3/EphA4 forward signaling, we performed two experiments. First, we cultured neurons
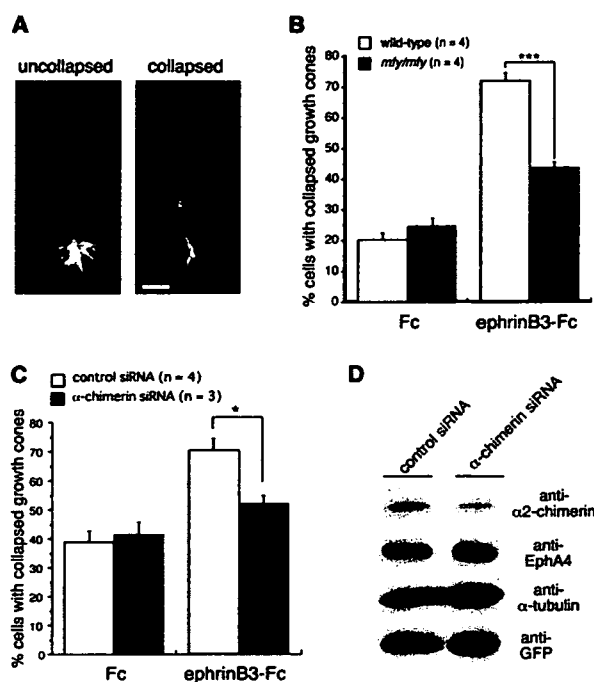
Figure 6. Downregulation of α-Chimerin Suppresses EphrinB3-Induced Growth Cone Collapse

(A) Representative examples of growth cones in phalloidin-stained cultured cortical neurons treated with preclustered Fc control (uncollapsed) or ephrinB3-Fc (collapsed). Scale bar: 10 μm.

(B) Growth cone collapse was induced by ephrinB3 in cultured neurons derived from the WT motor cortex, but was barely seen in those derived from the mfy/mfy cortex. All data are presented as the mean ± SEM of four independent experiments in each of which 100 neurons were counted (***$p < 0.001$, Student's t test).

(C) Downregulation of α-chimerin by siRNA suppressed ephrinB3-induced growth cone collapse in cultured cortical neurons. Cultured neurons derived from E18.5 rat cortex were transfected with a plasmid expressing both siRNA and enhanced yellow fluorescent protein (EYFP). In each experiment, 34–67 neurons expressing EYFP were counted. (*$p < 0.05$, Student's t test).

(D) α-chimerin-specific siRNA reduced the level of α-chimerin protein but not EphA4 protein. A 58.5% reduction of α-chimerin protein was observed in total lysates from cultured neurons in which 62% (not shown) of cells expressed α-chimerin-specific siRNA/EYFP, suggesting a drastic (>90%) reduction of α-chimerin.

derived from the motor cortex of WT and mfy/mfy mice on embryonic day 16.5 (E16.5) and then stimulated them with preclustered Fc or ephrinB3-Fc. EphrinB3 efficiently induced growth cone collapse in WT cortical neurons, as previously reported (Kullander et al., 2001a; Figures 6A and 6B); however, in the mfy/mfy cortical neurons, the frequency of collapse was significantly reduced (Figure 6B). Second, we expressed α-chimerin-specific siRNA by transfecting an expression vector into cultured neurons derived from the E18.5 rat motor cortex (Figure S8). The frequency of ephrinB3-induced growth cone collapse was significantly reduced in transfected neurons (Figure 6C), and western blotting with the anti-α2-chimerin antibody demonstrated that α-chimerin protein levels were

drastically reduced (>90%) in the transfected neurons (Figure 6D). We concluded that α-chimerin Rac-GAP acts downstream of ephrinB3/Eph signaling to cause growth cone collapse of cortical neurons.

Taken together, the results of our in vivo and in vitro studies confirm that α-chimerin Rac-GAP is a key molecule linking ephrinB3-induced EphA4 activation to the inactivation of Rac—a positive regulator of process outgrowth—thereby causing growth cone retraction and, eventually, axonal repulsion at the spinal cord midline.

DISCUSSION

α-Chimerin Is a Key Mediator of EphrinB3/EphA4 Forward Signaling and Causes Repulsion of CST Axons at the Spinal Cord Midline

We have shown the following. First, α-chimerin is colocalized with EphA4 in the developing CST (Figure S7). Second, it interacts with EphA4 both in vitro and in vivo (Figures 5A–5D). Third, when EphA4 is stimulated by ephrinB3, α-chimerin inactivates Rac, which is a positive regulator of process outgrowth, in vitro (Figure 5F). Fourth, ephrinB3-induced growth cone collapse is suppressed in cultured cortical neurons in which α-chimerin is downregulated by RNAi or mfy mutation (Figure 6). Fifth and finally, repulsion of CST axons at the spinal cord midline (Figures 1B and 4F) and formation of spinal CPGs (Figures 2C and 4G) are impaired in mfy/mfy mice and α-Chn KO mice, and both of these processes depend on ephrinB3/EphA4 forward signaling (Kullander et al., 2003, 2001a, 2001b; Yokoyama et al., 2001). Our results show that the Rac-GAP α-chimerin regulates CST axon guidance and CPG formation by mediating ephrinB3/EphA4 forward signaling (Figure 7).

It has been proposed that EphA receptors regulate growth cone dynamics through Rho-GEF ephexin1 (Shamah et al., 2001). During this process, activation of RhoA induces growth cone retraction and/or collapse, while activated Rac and Cdc42 promote its extension (Etienne-Manneville and Hall, 2002; Luo, 2000). The engagement of Ephs by ephrin leads to preferential activation of the exchange activity of ephexin toward RhoA, thus leading to growth cone collapse in vitro (Figure 7A; Shamah et al., 2001). We showed that the ephrin/Eph interaction leads to growth cone collapse due to Rac inactivation via the GAP activity of α-chimerin (Figure 7A). As both ephexin1 and α-chimerin are enriched in the central nervous system (Hall et al., 2001, 1993; Shamah et al., 2001), it is likely that the cooperative action of ephexin1-induced RhoA activation and α-chimerin-induced Rac inactivation function to induce retraction of growth cones during axon guidance in various circuits. Ephexin1 KO mice appear to be normal (Sahin et al., 2005). This absence of an obvious phenotype might be due to compensation by other ephexin family members. Alternatively, it might be due to the activity of α-chimerin, which could prevent growth cone extension by inactivating Rac in response to ephrin/Eph signaling, even in the absence of
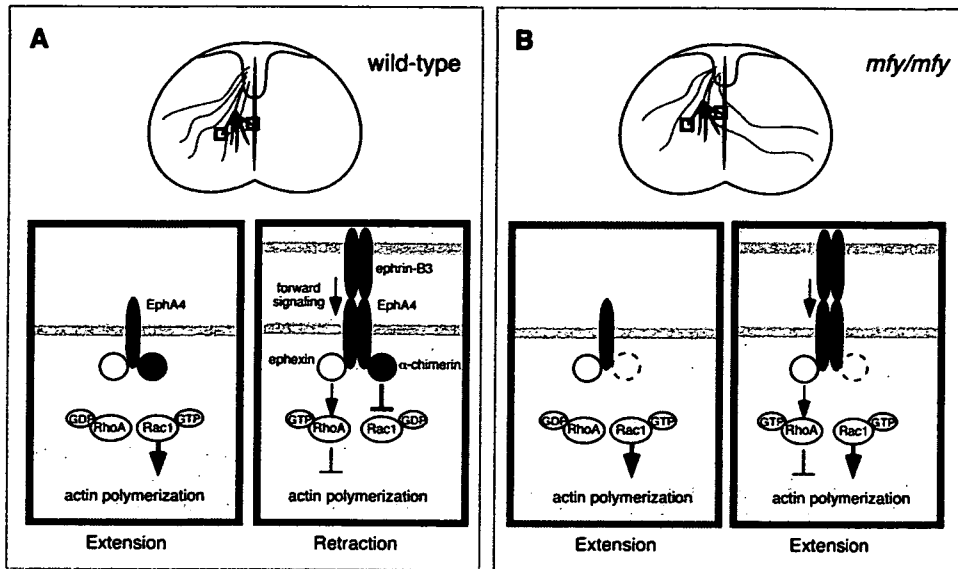
Figure 7. Model of EphrinB3/EphA4 Forward Signaling in Midline Repulsion of CST Axons

(A) In WT mice, the growth cones of CST axons extend due to basal activity of Rac, which is a positive regulator of process outgrowth, in the absence of ephrinB3 stimulation (green box). At the spinal cord midline that anchors ephrinB3, CST axons that express EphA4 receive forward signals. This ephrinB3/EphA4 forward signaling inactivates Rac through α-chimerin, leading to growth cone retraction (red box). Ephrin/EphA signaling might also activate RhoA, which is a negative regulator of process outgrowth, via ephexin (Shamah et al., 2001). The cooperative action of the RhoA-activator ephexin and the Rac-inactivator α-chimerin might induce efficient retraction of growth cones.

(B) In *mfy/mfy* mice, CST axons fail to stop at the midline due to the absence of α-chimerin-induced Rac inactivation, even in the presence of ephexin.

ephexin-induced RhoA activation. In contrast to the absence of an *Ephexin1* KO phenotype, we demonstrated that the formation of CST and CPGs is impaired in α-*Chn* mutant mice.

Critical Role of Rho-GTPase Inactivation in Ephrin/Eph Signaling

Ephrin/Eph signaling is important in a wide range of biological processes, including oocyte maturation, early morphogenesis, segmentation, guidance of migrating cells, synaptic plasticity, dendritic-spine formation, and axon guidance (Flanagan and Vanderhaeghen, 1998; Palmer and Klein, 2003; Pasquale, 2005). Recent studies of in vitro orientation suggest that in various biological phenomena, ephrin/Eph signaling regulates actin dynamics by activating Rho-GTPases, such as RhoA, Rac, and Cdc42, through Rho-GEFs (Cowan et al., 2005; Fu et al., 2007; Irie and Yamaguchi, 2002; Murai and Pasquale, 2005; Ogita et al., 2003; Penzes et al., 2003; Shamah et al., 2001; Tanaka et al., 2004). We suggest that a further mode of ephrin/Eph signaling exists, in which Ephs regulate actin dynamics by inactivating Rho-GTPases through Rho-GAPs.

Ephrin/Eph signaling might control actin dynamics by regulating the balance between negative regulators of actin polymerization (such as RhoA) and positive regulators (such as Rac and Cdc42; Sahin et al., 2005; Shamah et al., 2001). This theory only takes into account Rho-activation; however, we have now shown that Rho-inactiva-

tion is another important aspect of the ephrin/Eph regulation of actin dynamics. The activity of each Rho-GTPase might be controlled by the balance between its activation by Rho-GEFs and its inactivation by Rho-GAPs. In mammalian cells, there are many diverse Rho-GEFs and Rho-GAPs with different substrate specificities that are controlled by different mechanisms (Etienne-Manneville and Hall, 2002). Thus, it is possible that ephrin/Eph signaling in different processes employs specific Rho-GEFs and/or Rho-GAPs to achieve the appropriate balance of activity of each Rho-GTPase. In short, we propose that ephrin/Eph signaling regulates actin dynamics in two ways: first, by regulating the balance between the activities of different Rho-GTPases (such as RhoA and Rac or Cdc42), and second, by regulating the balance between activation and inactivation of each individual Rho-GTPase.

Regulation and Roles of α-Chimerin in Neural Development and Function

The present study provides evidence for the involvement of α-chimerin in ephrinB3/EphA4 forward signaling. How does ephrinB3/EphA4 signaling activate α-chimerin? As the kinase-inactive EphA4[FF] mutant protein could not activate α-chimerin (Figure 5F), it appeared that the kinase activity of EphA4 was necessary for the activation of α-chimerin. However, EphA4 kinase activity alone did not appear to be sufficient as the EphA4 proteins over-expressed in COS cells were phosphorylated and, thus,

kinase active, but were unable to fully activate α-chimerin in the absence of ephrinB3 stimulation (Figures 5E and 5F). In fact, it has been shown that the kinase activity of EphA4 alone is not sufficient for ephrinB/EphA4 forward signaling in vivo: the $EphA4^{EE/EE}$ mouse, the kinase of which is constitutively activated, has a normal alternate gait, normal CST axon midline guidance, normal CPG midline guidance, and normal morphology of the spinal cord (Egea et al., 2005). Cultured cortical neurons derived from $EphA4^{EE/EE}$ mice undergo normal growth cone collapse in response to clustered ephrinB3. Based on these observations, it has been proposed that higher-order clustering of EphA4 by stimulation of ephrinB is an essential component of ephrinB/EphA4 forward signaling (Egea et al., 2005). Our results are consistent with this idea.

Both the α1 and α2 isoforms of α-chimerin have a single copy of the C1 domain, which is a cysteine-rich motif, and can be activated by the binding of phorbol esters or diacylglycerol (DAG) to the C1 domain (Hall et al., 1990, 1993). Recently, it was reported that cyclin-dependent kinase 5 (Cdk5) regulates EphA4-mediated dendritic-spine retraction (Fu et al., 2007). Cdk5 is known to interact with α2-chimerin (Qi et al., 2004), so it is possible that a protein complex formed by clustering of EphA4 recruits some additional molecules required for linking activated EphA4 to α-chimerin activation. Such additional factors could include Cdk5/p35 and DAG-producing enzymes, such as phospholipase Cγ. It should be noted that these (or equivalent) factors do not appear to be specific to neurons, but rather are ubiquitous, as the expression of EphA4 and α2 isoforms in COS cells was sufficient to inactivate Rac upon stimulation by clustered-ephrinB3 (Figures 5E and 5F).

The α-Chn gene is widely expressed in the central nervous system both during development and in adulthood (Hall et al., 2001, 1990, 1993), and α-chimerin is found not only in axons but also in neuronal dendrites (Hall et al., 2001). It would be interesting to test whether α-chimerin plays a role in dendrite development in the brain. Recent studies using overexpression and/or siRNA-induced knockdown of α1-chimerin in cultured hippocampal neurons and cerebellar slices suggest that it regulates dendritic morphology and dendritic-spine density (Buttery et al., 2006; Van de Ven et al., 2005). α-chimerin might also be involved in NMDA receptor-dependent developmental plasticity, such as maturation of the barrel cortex (Iwasato et al., 2000, 1997), as well as in learning and memory, as it has been shown to interact with NMDA receptors in vitro (Van de Ven et al., 2005). The mfy/mfy mouse is thus a promising experimental model for elucidating the roles of α-chimerin Rac-GAP in the development and function of the central nervous system.

EXPERIMENTAL PROCEDURES

Animals
A Tg construct was made by modifying the RP23-413N9 BAC clone derived from B6 mouse genomic DNA (Roswell Park Cancer Institute,

NY, USA). The Tg founder mice were generated by microinjection of linearized constructs into fertilized eggs. α-Chn KO mice were generated using MS12 ES cells derived from the B6 strain (for details see the Supplemental Experimental Procedures). All of the mice were maintained according to the institutional guidelines of the animal facilities of the RIKEN-BSI.

VR Recordings
P1–P3 mice were anesthetized with isoflurane, and their spinal cords were removed as described elsewhere (Nishimaru et al., 2006). Electrical recordings of the VRs were made with glass-suction electrodes, and locomotor-like rhythmic activity was evoked by the concomitant bath application of NMDA (4–7 μM) and serotonin (5HT; 4–7 μM). Details of the recording procedure and data analyses are provided in the Supplemental Data.

Linkage Analyses
PCR primers for the microsatellite markers and SNPs were designed using the Mouse Genome Informatics (http://www.informatics.jax.org/) and National Centre for Biotechnology Information (http://www.ncbi.nlm.nih.gov/SNP/) databases, respectively, and were verified by PCR using the genomic DNAs of inbred B6 and DBA/2 mice and B6/DBA F_1 hybrids (for detailed methods, see Figure S3 and Supplemental Data).

Generation of Antibody
KLH-coupled synthetic peptides (MALTLFDTDEYRPPVWKC) corresponding to the N terminus of α2-chimerin (Figure S4A) were used to raise a rabbit polyclonal antibody (BSI Research Resources Center). Sera were affinity purified on the same peptides.

Measurement of Rac1 Activity
Transfected COS-7 cells were stimulated with 2 μg/ml preclustered ephrinB3-Fc (R&D Systems) in serum-free medium for 10 min. The cells were lysed with ice-cold cell lysis buffer containing 4 μg of GST-CRIB of αPak (amino acids 70–150). After centrifugation, the supernatant was incubated with glutathione-Sepharose beads, and bound proteins were analyzed by SDS–PAGE and immunoblotting (for detailed methods, see Supplemental Data).

Growth Cone Collapse Assay
Primary neurons were dissociated from the anterior dorsomedial to dorsal neocortex of E16.5 mice or E18.5 rats as described elsewhere (Ishikawa et al., 2003, Kullander et al., 2001a). The neurons were plated onto poly-D-lysine and laminin-coated coverslips and cultured in Neurobasal medium supplemented with 2% B27 (Invitrogen). They were then stimulated with 5 μg/ml preclustered ephrinB3-Fc for 30 min, fixed with 4% paraformaldehyde, and stained with rhodamine-conjugated phalloidin (Invitrogen; for detailed methods, see Supplemental Data).

Supplemental Data
Supplemental Data include Experimental Procedures, References, nine figures, and one table and can be found with this article online at http://www.cell.com/cgi/content/full/130/4/742/DC1/.

REFERENCES

Ahmed, S., Lee, J., Wen, L.P., Zhao, Z., Ho, J., Best, A., Kozma, R., and Lim, L. (1994). Breakpoint cluster region gene product-related domain of n-chimaerin. Discrimination between Rac-binding and GTPase-activating residues by mutational analysis. J. Biol. Chem. 269, 17642–17648.

Brown, M., Jacobs, T., Eickholt, B., Ferrari, G., Teo, M., Monfries, C., Qi, R.Z., Leung, T., Lim, L., and Hall, C. (2004). Alpha2-chimaerin, cyclin-dependent kinase 5/p35, and its target collapsin response mediator protein-2 are essential components in semaphorin 3A-induced growth-cone collapse. J. Neurosci. 24, 8994–9004.

Buttery, P., Beg, A.A., Chih, B., Broder, A., Mason, C.A., and Scheiffele, P. (2006). The diacylglycerol-binding protein alpha1-chimaerin regulates dendritic morphology. Proc. Natl. Acad. Sci. USA 103, 1924–1929.

Cowan, C.W., Shao, Y.R., Sahin, M., Shamah, S.M., Lin, M.Z., Greer, P.L., Gao, S., Griffith, E.C., Brugge, J.S., and Greenberg, M.E. (2005). Vav family GEFs link activated Ephs to endocytosis and axon guidance. Neuron 46, 205–217.

Diekmann, D., Brill, S., Garrett, M.D., Totty, N., Hsuan, J., Monfries, C., Hall, C., Lim, L., and Hall, A. (1991). Bcr encodes a GTPase-activating protein for p21rac. Nature 351, 400–402.

Dottori, M., Hartley, L., Galea, M., Paxinos, G., Polizzotto, M., Kilpatrick, T., Bartlett, P.F., Murphy, M., Kontgen, F., and Boyd, A.W. (1998). EphA4 (Sek1) receptor tyrosine kinase is required for the development of the corticospinal tract. Proc. Natl. Acad. Sci. USA 95, 13248–13253.

Egea, J., Nissen, U.V., Dufour, A., Sahin, M., Greer, P., Kullander, K., Mrsic-Flogel, T.D., Greenberg, M.E., Kiehn, O., Vanderhaeghen, P., et al. (2005). Regulation of EphA 4 kinase activity is required for a subset of axon guidance decisions suggesting a key role for receptor clustering in Eph function. Neuron 47, 515–528.

Eph Nomenclature Committee (1997). Unified nomenclature for Eph family receptors and their ligands, the ephrins. Cell 90, 403–404.

Etienne-Manneville, S., and Hall, A. (2002). Rho GTPases in cell biology. Nature 420, 629–635.

Flanagan, J.G., and Vanderhaeghen, P. (1998). The ephrins and Eph receptors in neural development. Annu. Rev. Neurosci. 21, 309–345.

Fu, W.Y., Chen, Y., Sahin, M., Zhao, X.S., Shi, L., Bikoff, J.B., Lai, K.O., Yung, W.H., Fu, A.K., Greenberg, M.E., et al. (2007). Cdk5 regulates EphA4-mediated dendritic spine retraction through an ephexin1-dependent mechanism. Nat. Neurosci. 10, 67–76.

Gianino, S., Stein, S.A., Li, H., Lu, X., Biesiada, E., Ulas, J., and Xu, X.M. (1999). Postnatal growth of corticospinal axons in the spinal cord of developing mice. Brain Res. Dev. Brain Res. 112, 189–204.

Grillner, S., and Wallen, P. (1985). Central pattern generators for locomotion, with special reference to vertebrates. Annu. Rev. Neurosci. 8, 233–261.

Hall, C., Monfries, C., Smith, P., Lim, H.H., Kozma, R., Ahmed, S., Vanniasingham, V., Leung, T., and Lim, L. (1990). Novel human brain cDNA encoding a 34,000 Mr protein n-chimaerin, related to both the regulatory domain of protein kinase C and BCR, the product of the breakpoint cluster region gene. J. Mol. Biol. 211, 11–16.

Hall, C., Sin, W.C., Teo, M., Michael, G.J., Smith, P., Dong, J.M., Lim, H.H., Manser, E., Spurr, N.K., Jones, T.A., et al. (1993). Alpha 2-chi-

merin, an SH2-containing GTPase-activating protein for the ras-related protein p21rac derived by alternate splicing of the human n-chimerin gene, is selectively expressed in brain regions and testes. Mol. Cell. Biol. 13, 4986–4998.

Hall, C., Michael, G.J., Cann, N., Ferrari, G., Teo, M., Jacobs, T., Monfries, C., and Lim, L. (2001). Alpha2-chimaerin, a Cdc42/Rac1 regulator, is selectively expressed in the rat embryonic nervous system and is involved in neuritogenesis in N1E–115 neuroblastoma cells. J. Neurosci. 21, 5191–5202.

Inoue, H., Tsukita, K., Iwasato, T., Suzuki, Y., Tomioka, M., Tateno, M., Nagao, M., Kawata, A., Saido, T.C., Miura, M., et al. (2003). The crucial role of caspase-9 in the disease progression of a transgenic ALS mouse model. EMBO J. 22, 6665–6674.

Irie, F., and Yamaguchi, Y. (2002). EphB receptors regulate dendritic spine development via intersectin, Cdc42 and N-WASP. Nat. Neurosci. 5, 1117–1118.

Ishikawa, Y., Katoh, H., and Negishi, M. (2003). A role of Rnd1 GTPase in dendritic spine formation in hippocampal neurons. J. Neurosci. 23, 11065–11072.

Iwasato, T., Erzurumlu, R.S., Huerta, P.T., Chen, D.F., Sasaoka, T., Ulupinar, E., and Tonegawa, S. (1997). NMDA receptor-dependent refinement of somatotopic maps. Neuron 19, 1201–1210.

Iwasato, T., Datwani, A., Wolf, A.M., Nishiyama, H., Taguchi, Y., Tonegawa, S., Knopfel, T., Erzurumlu, R.S., and Itohara, S. (2000). Cortex-restricted disruption of NMDAR1 impairs neuronal patterns in the barrel cortex. Nature 406, 726–731.

Kiehn, O., and Kullander, K. (2004). Central pattern generators deciphered by molecular genetics. Neuron 41, 317–321.

Kullander, K., Croll, S.D., Zimmer, M., Pan, L., McClain, J., Hughes, V., Zabski, S., DeChiara, T.M., Klein, R., Yancopoulos, G.D., et al. (2001a). Ephrin-B3 is the midline barrier that prevents corticospinal tract axons from recrossing, allowing for unilateral motor control. Genes Dev. 15, 877–888.

Kullander, K., Mather, N.K., Diella, F., Dottori, M., Boyd, A.W., and Klein, R. (2001b). Kinase-dependent and kinase-independent functions of EphA4 receptors in major axon tract formation in vivo. Neuron 29, 73–84.

Kullander, K., Butt, S.J., Lebret, J.M., Lundfald, L., Restrepo, C.E., Rydstrom, A., Klein, R., and Kiehn, O. (2003). Role of EphA4 and EphrinB3 in local neuronal circuits that control walking. Science 299, 1889–1892.

Liang, F.Y., Moret, V., Wiesendanger, M., and Rouiller, E.M. (1991). Corticomotoneuronal connections in the rat: evidence from double-labeling of motoneurons and corticospinal axon arborizations. J. Comp. Neurol. 311, 356–366.

Luo, L. (2000). Rho GTPases in neuronal morphogenesis. Nat. Rev. Neurosci. 1, 173–180.

Murai, K.K., and Pasquale, E.B. (2005). New exchanges in eph-dependent growth cone dynamics. Neuron 46, 161–163.

Nishimaru, H., and Kudo, N. (2000). Formation of the central pattern generator for locomotion in the rat and mouse. Brain Res. Bull. 53, 661–669.

Nishimaru, H., Restrepo, C.E., and Kiehn, O. (2006). Activity of Renshaw cells during locomotor-like rhythmic activity in the isolated spinal cord of neonatal mice. J. Neurosci. 26, 5320–5328.

Noren, N.K., and Pasquale, E.B. (2004). Eph receptor-ephrin bidirectional signals that target Ras and Rho proteins. Cell. Signal. 16, 655–666.

Ogita, H., Kunimoto, S., Kamioka, Y., Sawa, H., Masuda, M., and Mochizuki, N. (2003). EphA4-mediated Rho activation via Vsm-RhoGEF expressed specifically in vascular smooth muscle cells. Circ. Res. 93, 23–31.

Palmer, A., and Klein, R. (2003). Multiple roles of ephrins in morphogenesis, neuronal networking, and brain function. Genes Dev. *17*, 1429–1450.

Pasquale, E.B. (2005). Eph receptor signalling casts a wide net on cell behaviour. Nat. Rev. Mol. Cell Biol. *6*, 462–475.

Penzes, P., Beeser, A., Chernoff, J., Schiller, M.R., Eipper, B.A., Mains, R.E., and Huganir, R.L. (2003). Rapid induction of dendritic spine morphogenesis by trans-synaptic ephrinB-EphB receptor activation of the Rho-GEF kalirin. Neuron *37*, 263–274.

Qi, R.Z., Ching, Y.P., Kung, H.F., and Wang, J.H. (2004). Alpha-chimerin exists in a functional complex with the Cdk5 kinase in brain. FEBS Lett. *561*, 177–180.

Sahin, M., Greer, P.L., Lin, M.Z., Poucher, H., Eberhart, J., Schmidt, S., Wright, T.M., Shamah, S.M., O'Connell, S., Cowan, C.W., et al. (2005). Eph-dependent tyrosine phosphorylation of ephexin1 modulates growth cone collapse. Neuron *46*, 191–204.

Shamah, S.M., Lin, M.Z., Goldberg, J.L., Estrach, S., Sahin, M., Hu, L., Bazalakova, M., Neve, R.L., Corfas, G., Debant, A., et al. (2001). EphA receptors regulate growth cone dynamics through the novel guanine nucleotide exchange factor ephexin. Cell *105*, 233–244.

Tanaka, M., Ohashi, R., Nakamura, R., Shinmura, K., Kamo, T., Sakai, R., and Sugimura, H. (2004). Tiam1 mediates neurite outgrowth induced by ephrin-B1 and EphA2. EMBO J. *23*, 1075–1088.

Van de Ven, T.J., VanDongen, H.M., and VanDongen, A.M. (2005). The nonkinase phorbol ester receptor alpha1-chimerin binds the NMDA receptor NR2A subunit and regulates dendritic spine density. J. Neurosci. *25*, 9488–9496.

Wahl, S., Barth, H., Ciossek, T., Aktories, K., and Mueller, B.K. (2000). Ephrin-A5 induces collapse of growth cones by activating Rho and Rho kinase. J. Cell Biol. *149*, 263–270.

Whelan, P., Bonnot, A., and O'Donovan, M.J. (2000). Properties of rhythmic activity generated by the isolated spinal cord of the neonatal mouse. J. Neurophysiol. *84*, 2821–2833.

Yokoyama, N., Romero, M.I., Cowan, C.A., Galvan, P., Helmbacher, F., Charnay, P., Parada, L.F., and Henkemeyer, M. (2001). Forward signaling mediated by ephrin-B3 prevents contralateral corticospinal axons from recrossing the spinal cord midline. Neuron *29*, 85–97.

ELSEVIER

Pael receptor is involved in dopamine metabolism in the nigrostriatal system

Yuzuru Imai [a,1,*], Haruhisa Inoue [a,1,2], Ayane Kataoka [a], Wang Hua-Qin [a,2], Masao Masuda [c],
Toshio Ikeda [b], Kayoko Tsukita [a], Mariko Soda [a], Tohru Kodama [d], Tatsu Fuwa [e],
Yoshiko Honda [d], Satoshi Kaneko [f], Sadayuki Matsumoto [f], Kazumasa Wakamatsu [g],
Shosuke Ito [g], Masami Miura [c], Toshihiko Aosaki [c],
Shigeyoshi Itohara [b], Ryosuke Takahashi [a,**]

[a] *Laboratory for Motor System Neurodegeneration, RIKEN Brain Science Institute (BSI), Saitama 351-0198, Japan*
[b] *Laboratory for Behavioral Genetics, RIKEN Brain Science Institute (BSI), Saitama 351-0198, Japan*
[c] *Neural Circuits Dynamics Research Group, Tokyo Metropolitan Institute of Gerontology, Tokyo 173-0015, Japan*
[d] *Department of Psychology, Tokyo Metropolitan Institute for Neuroscience, Tokyo 183-8526, Japan*
[e] *Department of Neurology, Tokyo Metropolitan Institute for Neuroscience, Tokyo 183-8526, Japan*
[f] *Department of Neurology, Kitano Hospital, The Tazuke Kofukai Medical Research Institute, Osaka 530-8480, Japan*
[g] *Department of Chemistry, Fujita Health University School of Health Sciences, Aichi 470-1192, Japan*

Abstract

Pael receptor (Pael-R) has been identified as one of the substrates of Parkin, a ubiquitin ligase responsible for autosomal recessive juvenile Parkinsonism (AR-JP). When Parkin is inactivated, unfolded Pael-R accumulates in the endoplasmic reticulum and results in neuronal death by unfolded protein stress, suggesting that Pael-R has an important role in the pathogenesis of AR-JP. Here we report the analyses on Pael-R-deficient (KO) and Pael-R-transgenic (Tg) mice. The striatal dopamine (DA) level of Pael-R KO mice was only 60% of that in normal mice, while in Pael-R Tg mice, striatal 3,4-dihydroxyphenylacetic acid (DOPAC) as well as vesicular DA content increased. Moreover, the nigrostriatal dopaminergic neurons of Pael-R Tg mice are more vulnerable to Parkinson's disease-related neurotoxins while those of Pael-R KO mice are less. These results strongly suggest that the Pael-R signal regulates the amount of DA in the dopaminergic neurons and that excessive Pael-R expression renders dopaminergic neurons susceptible to chronic DA toxicity.
© 2007 Elsevier Ireland Ltd and the Japan Neuroscience Society. All rights reserved.

Keywords: Parkinson's disease; Parkin; Striatum; Substantia nigra; AR-JP; GPR37; MPTP; 6-OHDA

1. Introduction

* Corresponding author. Present address: Institute of Development, Aging and Cancer, Tohoku University, Sendai 980-8575, Japan. Tel.: +81 22 717 8490; fax: +81 22 717 8490.
** Corresponding author. Present address: Department of Neurology, Kyoto University School of Medicine, Kyoto 606-8507, Japan. Tel.: +81 75 751 3770; fax: +81 75 761 9780.
E-mail addresses: yimai@idac.tohoku.ac.jp (Y. Imai), ryosuket@kuhp.kyoto-u.ac.jp (R. Takahashi).
[1] These authors contributed equally to this work.
[2] Present address: Department of Neurology, Kyoto University School of Medicine, Kyoto 606-8507, Japan.

DA is one of the important neurotransmitters of the central nervous system (CNS). Animal studies reveal that increasing synaptic DA concentration by inhibiting DA transporters or blocking DA autoreceptors stimulates locomotion and exploratory behavior. Conversely, blocking DA receptors attenuates the effects of food rewards, intracranial self-stimulation, and psychomotor stimulants. DA-deficient animals show severe adipsia, aphagia, hypoactivity, and impaired complicated motor behaviors (Zhou and Palmiter, 1995). About 75% of the dopaminergic neurons in the brain have their cell bodies in the substantia nigra (SN) of the basal ganglia and project to

the striatum. Progressive loss of this population underlies Parkinson's disease (PD) in humans (Betarbet et al., 2002). Most cases of PD are sporadic and the etiology of common PD remains unknown. However, recent identification of gene mutations in familial cases of PD has advanced our understanding of the molecular mechanisms behind the neurodegeneration associated with this disease.

A major cause of juvenile PD, autosomal recessive juvenile Parkinsonism (AR-JP), results from mutations in the Parkin gene (Kitada et al., 1998). Parkin protein is a RING-finger type ubiquitin ligase (E3) and AR-JP-linked Parkin mutants are defective in E3 activity (Imai et al., 2000; Shimura et al., 2000; Zhang et al., 2000). The accumulation of unfolded Pael-R, a substrate for Parkin recently identified in our laboratory, causes unfolded protein stress, which results in cell death *in vivo* and *in vitro* (Imai et al., 2001; Yang et al., 2003). Parkin eliminates unfolded Pael-R in cooperation with the molecular chaperone Hsp70 and a U box protein known as CHIP (Imai et al., 2002). Pael-R, which is abundantly expressed in dopaminergic neurons of the SN, other regions (such as the hippocampus), and some nuclei of the brainstem and in oligodendrocytes, is a putative G protein coupled receptor whose ligand is unknown (Donohue et al., 1998; Imai et al., 2001) and whose physiological function in the brain remains unclear.

Here we provide genetic evidence in mice that Pael-R is involved in the regulation of nigrostriatal dopamine metabolism and propose a hypothesis of DA neuron-specific pathological mechanism by Pael-R expression.

2. Materials and methods

2.1. Targeted disruption of the mouse Pael-R gene

Pael-R KO mouse was generated by standard technique of gene targeting (Gomi et al., 1995). A targeting vector was constructed using 17.5-kb genomic DNA fragments containing exon 1 of Pael-R gene (Fig. 1C). Floxed pgk-neo cassette and loxP sequence were inserted at the sites of the intron 1 and untranslated region of exon 1, respectively. DT-ApA cassette was flanked at 5' end of homologous arm for negative selection (Yanagawa et al., 1999). The linearized targeting vector was transfected into MS12 (C57BL/6J [B6]) ES cells. Positive clones were selected by Southern blots analysis, and then injected into Balb/c blastcysts. Offsprings harboring targeted allele were generated from the crossing of chimera mice with B6 mice and confirmed by Southern blots analysis. To generate a null allele, B6 eggs *in vitro* fertilized by F1 sperm were microinjected with circular plasmid DNA containing the Cre recombinase gene as described previously (Sunaga et al., 1997). After the confirmation of null allele by Southern blots analysis, heterozygous mice harboring null allele were intercrossed for obtaining the homozygous mice as Pael-R KO mice.

2.2. Generation of Pael-R Tg mice

Human platelet-derived growth factor β2 promoter-driven human Pael-R transgenic (PDGFβ-Tg) mice, and mouse prion protein promoter-driven Pael-R Tg (PrP-Tg) mice were generated using the human PDGF β2 vector (Chui et al., 1999) (kindly provided by Drs. Tanahashi H. and Tabira T., National Institute of Neuroscience, Japan), and MoPrP vector (Borchelt et al., 1996) (kindly provided by Drs. Borchelt D.R. and Fromholt D., Johns Hopkins University). The NotI fragments from the PDGFβ-Pael-R and the PrP-Pael-R plasmids were microinjected into B6 and C3H/B6 mouse eggs, respectively. Potential founders were identified using Southern blot analysis and PCR. Stable Tg lines were established by breeding founders to B6 mice (for PDGFβ-Tg) and C3H/B6 mice (for PrP-Tg).

2.3. Antibodies

Anti-Pael-R (#202) and anti-LP-2 (#23) monoclonal antibodies (mAbs) were raised in mice against the C-terminal 61 amino acids of human Pael-R and the C-terminal 62 amino acids of human ETbR-LP2 (LP-2), respectively, expressed in bacteria. Anti-TH (MAB318) and anti-actin (MAB1501R) Abs were purchased from Chemicon. Anti-transferrin receptor (H68.4) and anti-NSE (BBS/NC/VI-H14) Abs were obtained from Zymed and Dako, respectively.

2.4. Western blots and immunohistochemistry

A crude homogenate was prepared by adding 10 µl of ice-cold buffer A (50 mM Tris-HCl, pH 7.5, 120 mM NaCl, 5 mM EDTA containing Complete Protease Inhibitors [Roche Diagnostics])/mg of brain tissue and using a Dounce homogenizer with a tight pestle (40 strokes). The suspension was fractionated by centrifugation at 1000 × g for 5 min and then by ultracentrifugation at 165,000 × g for 60 min. The pellet fraction was washed three times with buffer A, and then extracted by shaking in 5 µl of buffer B (buffer A containing 1% Triton X-100 and 1% SDS)/mg of brain tissue for 60 min at RT. After centrifugation at 18,500 × g for 30 min, the pooled supernatants were used as the total membrane fraction. Each fraction was Western blotted using ECL detection reagents (GE Healthcare). Protein was quantified using the Coomassie protein assay reagent (Pierce).

2.5. Animal treatment, drugs, and behavior

Three-month-old male littermates of heterozygous interbreedings were used in the 1-methyl-4-phenyl-1,2,3,6-tetrahydropyridine (MPTP) experiments. Mice received either two intraperitoneal injections of MPTP (Sigma; 10 h apart; 30 mg/kg each), or vehicle control (saline). The animal experiments described were approved by Animal Experiments Committee of RIKEN Brain Science Institute. All procedures were performed according to guidelines of RIKEN Brain Science Institute. Treatment with 6-hydroxydopamine (6-OHDA) was performed as described previously (Kaneko et al., 2000). In short, the male Tg or KO mice at 2–3 months of age and their littermates were deeply anesthetized with sodium pentobarbital (50 mg/kg i.p.). A needle was introduced into the left hemisphere using stereotaxic techniques, and phosphate-buffered saline (PBS, 0.5 µl) containing 6-OHDA hydrobromide (4 mg/ml) and 0.016% ascorbic acid was injected into two sites in the left striatum over 5 min. After 1 week (for the MPTP experiments) and 3 weeks (for the 6-OHDA experiments), mice were subjected to neurochemical analysis or counting of the number of tyrosine hydroxylase (TH)-positive neurons as follows. The brain perfused with cold PBS followed by 4% paraformaldehyde in PBS, was removed, embedded in paraffin, sectioned (12 µm), deparaffinized using standard protocols, and stained with anti-TH mAb (Chemicon, 1:100). The total number of TH-stained cells with clearly visible nuclear borders in the substantia nigra pars compacta was estimated in every fifth section, using a previously described unbiased stereological method (Nelson et al., 1996; West, 1999). A complete reduction of TH immunosignal in the striatum was also used to confirm that the injection sites of each animal were optimally located. For spontaneous locomotion activities, mice were placed in white chambers (50 cm × 50 cm). After introduction of mice without acclimation, horizontal migration up to 30 min was recorded by overhead CCD cameras and analyzed by Image OF4, a program based on the NIH image program (O'Hara & Co. Ltd., Tokyo, Japan).

2.6. Neurochemical analysis

Striatal tissue was homogenized in solution H (0.4 M HClO₄ containing 4 mM Na₂S₂O₅, 4 mM diethylenetriaminepentaacetic acid and 5 mM 1,4-dithiothreitol). The supernatant by centrifugation at 18,500 × g for 10 min was used for measurement of free catechols. The alumina extraction of free catechols was basically performed as described previously (Ito et al., 1988).

2.7. In vivo microdialysis

Mice were anesthetized with sodium pentobarbital and placed in a stereotaxic frame. Dialysis probes (membrane length, 2.0 mm; outer diameter,
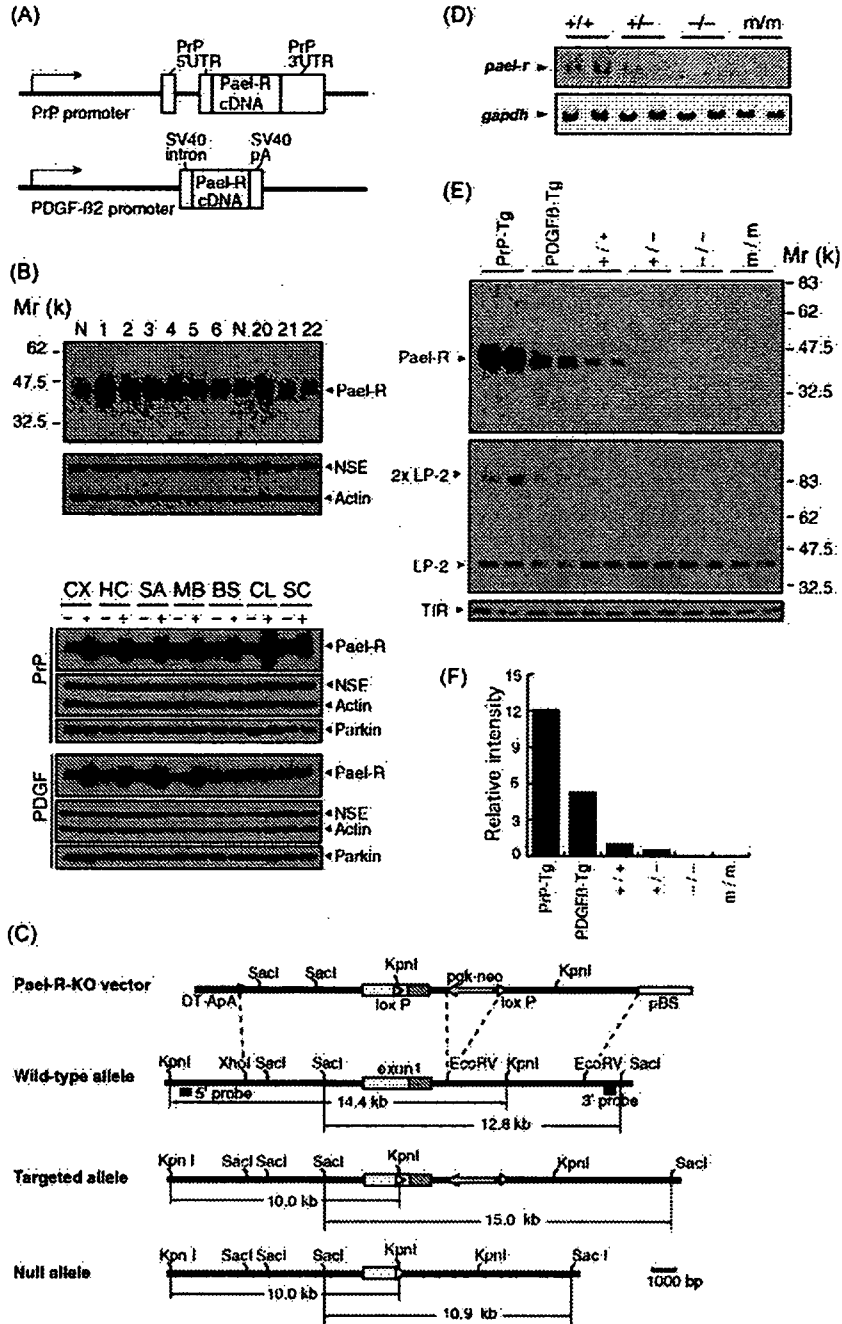
Fig. 1. Generation of Pael-R Tg and Pael-R KO mice. (A) Expression of the Pael-R gene was under the control of the PrP and PDGF β2 promoter. pA, polyadenylation sequence. (B) Expression levels of Pael-R in the whole brain of each PrP-Tg line (1–6), PDGFβ-Tg (20–22) and non-Tg mouse (N) are shown (upper). Expression levels of Pael-R and Parkin in each region of the brain of PrP-Tg line 1 and PDGFβ-Tg line 20 mice and their non-Tg littermates (lower). CX, cerebral cortex; HC, hippocampus; SA, striatum; MB, midbrain; BS, pons and medulla; CL, cerebellum, and SC, spinal cord. The amounts of neuron-specific enolase (NSE) and actin in each lane were shown as loading controls. (C) The murine Pael-R gene and targeting vector. A region of the Pael-R gene that includes the proximal exon 1 with a start codon is shown. Two loxP sites were inserted on the both sides of the Pael-R coding region within exon 1 (5′-UTR, white box; CDS1, gray box; a loxP site in the exon 1, 461 bp upstream from the translation initiation site). A *neo* cassette was inserted after exon 1. Locations of probes for southern blot analysis are indicated. DT-ApA, the diphtheria toxin gene with poly(A) sequence for negative selection; pBS, pBluescript (Stratagene). (D) Northern blot analysis of Pael-R transcripts (*pael-r*) in representative brain samples. '+', '−', and 'm' indicates the WT, null and targeted allele in (C), respectively. The same blot was hybridized with a *gapdh* probe as a loading control (*gapdh*). (E) Western blot analysis with the membrane fractions from the whole brain of 2.5-month-old mice. LP-2, ETβR-LP2; 2× LP-2, a putative SDS-resistant dimer form of LP2; TfR, transferrin receptor. (F) Quantitative analysis of expression levels of Pael-R protein normalized against each TfR level in (E). The mean amounts of Pael-R in WT (+/+) are defined as one.

0.22 mm; D-I-6-02, Eicom, Kyoto, Japan) were implanted in the left striatum. The stereotaxic coordinates for implantation of microdialysis probes were anterior–posterior, 0.26 mm; dorsal–ventral, 3.5 mm; and lateral, 2.0 mm relative to the bregma (Goldberg et al., 2003). Placement of the probe was verified by histological examination subsequent to the experiments. Following surgery, animals were returned to their home cages and given free access to food and water. Twenty hours later, to avoid transient changes, if any, caused by surgical damage, the dialysis probe was connected to a syringe pump and

perfusion was carried out at 1.0 μl/min with artificial striatal cerebrospinal fluid (aCSF: Na$^+$, 155.0 mM; Ca^{2+}, 1.1 mM; K$^+$, 2.9 mM; Mg^{2+}, 0.8 mM; and Cl$^-$, 155.6 mM; pH 7.4). After a 4-h equilibration period, the perfusates were collected every 30 min. The basal level of DA was determined by averaging the DA levels of eight dialysates collected during a 4-h period. The DA level due to Ca^{2+}-dependent efflux was the difference between the basal level and the average level in two consecutive dialysates collected within 1 h after perfusion of Ca^{2+}-free aCSF for 2 h. Samples were assayed for DA or DOPAC using HPLC-EC.

2.8. Electrophysiology

The midbrain slices and corticostriatal slices prepared from 3–4-week-old mice were cut coronally and parasagittally, respectively (250 μm thick), transferred to an incubation chamber and allowed to recover for 1 h before recording. During recording, a slice was perfused continuously with aCSF (124 mM NaCl, 3 mM KCl, 1 mM NaH$_2$PO$_4$, 1.2 mM MgCl$_2$, 2.4 mM CaCl$_2$, 10 mM glucose, 26 mM NaHCO$_3$, pH 7.4) saturated with 95% O$_2$, and 5% CO$_2$ at a rate of 1–2 ml/min at 30 °C. Whole-cell patch-clamp recordings were made from DA neurons in midbrain slices or striatal medium spiny neurons (MSNs) in corticostriatal slices by an EPC9/2 amplifier (HEKA Elektronik Lambrecht/Pfalz, Germany) with infrared differential contrast visualization using an Olympus BX50WI (Tokyo, Japan) and a CCD camera. For current-clamp recordings, patch pipettes contained 129 mM K-gluconate, 11 mM KCl, 2 mM MgCl$_2$, 10 mM HEPES, 4 mM Na$_2$-ATP, 0.3 mM GTP, and 0.5%

biocytin (brought to pH 7.3 with KOH; osmolarity 280 mOsm). Hyperpolarizing and depolarizing current injection was made to study the physiological properties of DA neurons. For voltage-clamp recordings, patch pipettes (4–6 MΩ) were filled with 124 mM Cs-methanesulfonate, 11 mM KCl, 2 mM MgCl$_2$, 10 mM HEPES, 4 mM Na$_2$-ATP, 0.3 mM GTP, 0.1 mM spermine, 5 mM QX-314, and 0.5% biocytin and brought to 280 mOsm and pH 7.3 with CsOH. Inhibitory postsynaptic currents (IPSCs) were evoked by electrical stimulation of the striatum with a bipolar tungsten electrode in the presence of the N-methyl-D-aspartate receptor antagonist D(−)-2-amino-5-phosphono-pentanoic acid (D-AP5, 25 μM) and the α-amino-3-hydroxy-5-methyl-4-isoxazolepropionic acid receptor antagonist 6-cyano-7-nitroquinoxaline-2,3-dione (CNQX, 20 μM). Effects of paired pulse stimulation were then investigated by delivering five pairs of stimuli at decreasing intervals (500, 200, 100, 50, and 25 ms). Thirty stimulus pulses given 70 ms apart (about 14 Hz) were next applied three times every 20 s. Nomifensine (3 μM), an uptake inhibitor of DA, was then bath-applied. Voltage errors attributable to the liquid junction potential (11 mV) were subtracted. Signals were filtered at 5 kHz and digitized at 20 kHz with Pulse/PulseFit (HEKA). If series resistance was changed by >20%, the experiments were discarded. To confirm the morphology of the recorded neurons, the slices containing biocytin-filled cells were fixed and stained with Vectastain ABC kit (Vector Laboratories). Areas of cell bodies of DA neurons were measured using NIH Image J software (http://rsb.info.nih.gov/ij/). Statistical significance was assessed by unpaired or paired Student's t-tests. D-AP5 was obtained from Tocris Cookson and all other drugs from Sigma.
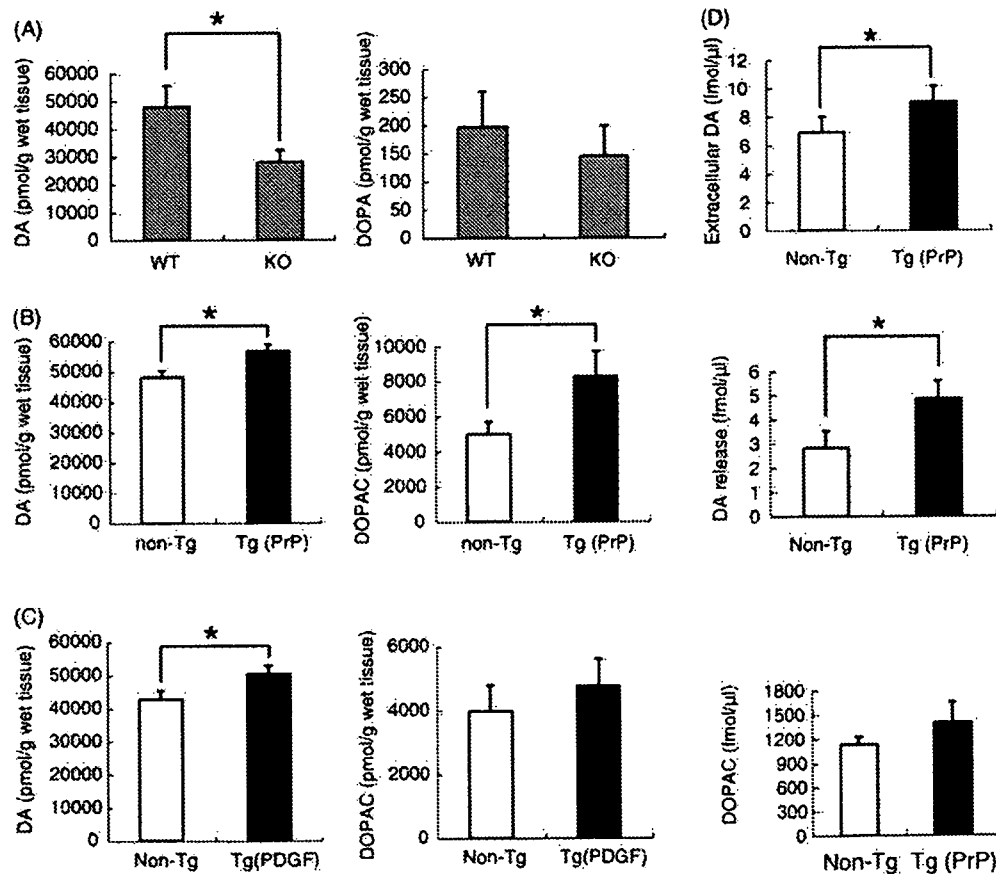

Fig. 2. DA and its metabolites in the striatum of Pael-R Tg and Pael-R KO mice. (A) Striatal tissue levels of DA (left) and L-DOPA (right) in Pael-R KO and WT littermate mice measured by HPLC-EC ($n = 6$ each). Results are presented as the mean ± S.E.M. for six animals at 13-months of age. *$P < 0.05$ vs. WT by Student's t-test. (B) Striatal tissue levels of DA and DOPAC in PrP-Tg and non-Tg littermate mice measured by HPLC-EC. Results are presented as the mean ± S.E.M. for 15 animals at 10-months of age. *$P < 0.05$ vs. non-Tg by Student's t-test. (C) Striatal tissue levels of DA and DOPAC in PDGFβ-Tg and non-Tg littermate mice measured by HPLC-EC. Results are presented as the mean ± S.E.M. for 12 animals at 15 months of age. *$P < 0.05$ vs. non-Tg by Student's t-test. (D) Extracellular DA levels (upper), DOPAC levels (lower), and Ca^{2+}-dependent DA release (middle) in the striatum of free moving PrP-Tg and non-Tg littermate mice at 10 months of age measured by microdialysis (mean ± S.E.M., $n = 10$ each). *$P < 0.05$ vs. non-Tg by Student's t-test.
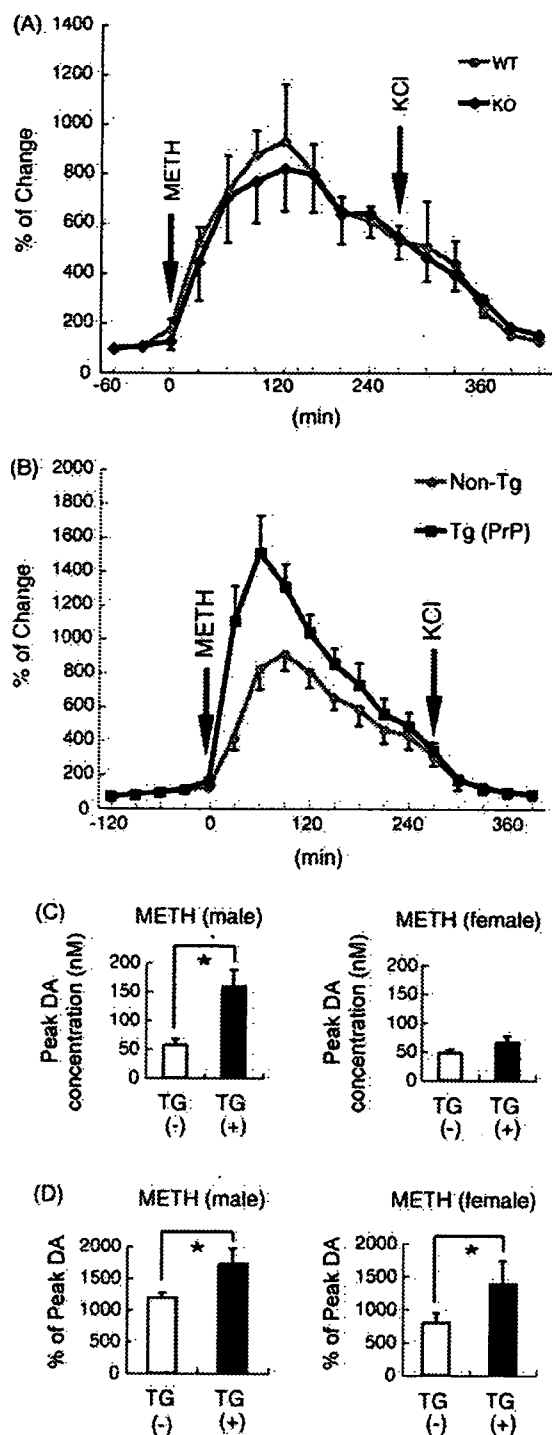
Fig. 3. Hypersensitivity to methamphetamine in Pael-R Tg mice. (A) Time course of DA release in the striatum of Pael-R KO ($n = 8$) and WT littermate mice ($n = 8$) in response to methamphetamine (METH, 30 mg/kg, s.c.). Perfusion of medium containing 100 mM KCl through the microdialysis probe at 270 min after METH stimulation did not show another peak of DA release, suggesting that almost all of the intracellular DA was released by this METH administration. The values are represented as the mean ± S.E.M. of percentage to basal levels (average of the levels at 30 and 60 min before METH administration) for eight animals at 6–12 months of age. (B) Time course of DA release in the striatum of PrP-Tg ($n = 10$) and non-Tg littermate mice ($n = 10$) in response to METH (30 mg/kg, s.c.) and subsequent KCl (100 mM) administration as in (A). The values for 10 animals at 6 months of age are represented as in (A). DA release after METH stimulation in PrP-Tg was significantly different by repeated measures ANOVA [genotype × time interaction, $F_{(1,245)} = 27.1$;

3. Results

3.1. Generation of Pael-R Tg and Pael-R KO mice

Tg mice were generated expressing human Pael-R under the control of the PrP promoter and the PDGF β2 promoter (Fig. 1A). Several lines of Tg mice were obtained, and mice with the highest expression levels of Pael-R were chosen from each promoter group and characterized (Fig. 1B). The PrP promoter-driven transgenic (PrP-Tg) line PrP1 (maintained on a mixed genetic background of C3H × B6), showed high expression of Pael-R transgene in the whole brain, while the PDGF β2 promoter-driven transgenic (PDGFβ-Tg) line 20 on a B6 background showed marked expression in the striatum and the midbrain compared with other regions (Fig. 1B). The expression of Pael-R transgene in TH-positive neurons in the SN was immunohistochemically confirmed by increased Pael-R immunosignals compared with that of non-Tg mice (data not shown).

Murine Pael-R gene contains two exons (Marazziti et al., 1998). The first exon containing a start codon was targeted to generate Pael-R-deficient mice on a B6 background. Two loxP sites flanking exon 1 and a selection marker cassette were introduced into the mouse Pael-R gene by means of homologous recombination in ES cells (Fig. 1C, targeted allele). To generate a null allele, part of the exon 1 and the selection marker were removed by in vitro fertilization using sperm from a heterozygote mouse bearing the targeted allele and subsequent microinjection of Cre recombinase cDNA into the fertilized eggs. Homologous recombination of the targeting construct and the deletion of the floxed cassette were confirmed by Southern blotting (data not shown). To determine the level of expression of Pael-R transcripts, Northern blotting analysis was performed with total RNA from whole brain samples (Fig. 1D). This analysis indicated that in mice carrying both the targeted and null alleles, the expression of Pael-R mRNA transcripts is completely lost, suggesting that the insertion of loxP or the selection cassette on non-coding regions has disrupted a critical element(s) for transcripton.

The protein levels of expression in Pael-R Tg and KO mice were assessed by Western blotting with membrane fractions prepared from whole brain of samples with anti-Pael-R Ab (Fig. 1E). PrP-Tg and PDGFβ-Tg mice had respectively ~12 and ~5.5 times higher Pael-R protein levels compared with normal mice (+/+), while homozygote mice bearing the null allele or targeted allele failed to show an immunosignal of the Pael-R protein (Fig. 1E and F) The alterations of Pael-R expression had no effect on the expression of LP-2, whose gene has the highest homology with the Pael-R gene (Fig. 1E) (Valdenaire et al., 1998).

$P < 0.001$]. (C) The peak values of striatal DA efflux after METH treatment in PrP-Tg male (left, $n = 5$ each group) and female (right, $n = 5$ each group) mice are shown. $*P < 0.05$ vs. non-Tg by Student's t-test. (D) Percent of the peak DA efflux to basal DA content after METH treatment in PrP-Tg male (left, $n = 5$ each group) and female (right, $n = 5$ each group) mice is shown. $*P < 0.05$ vs. non-Tg by Student's t-test.
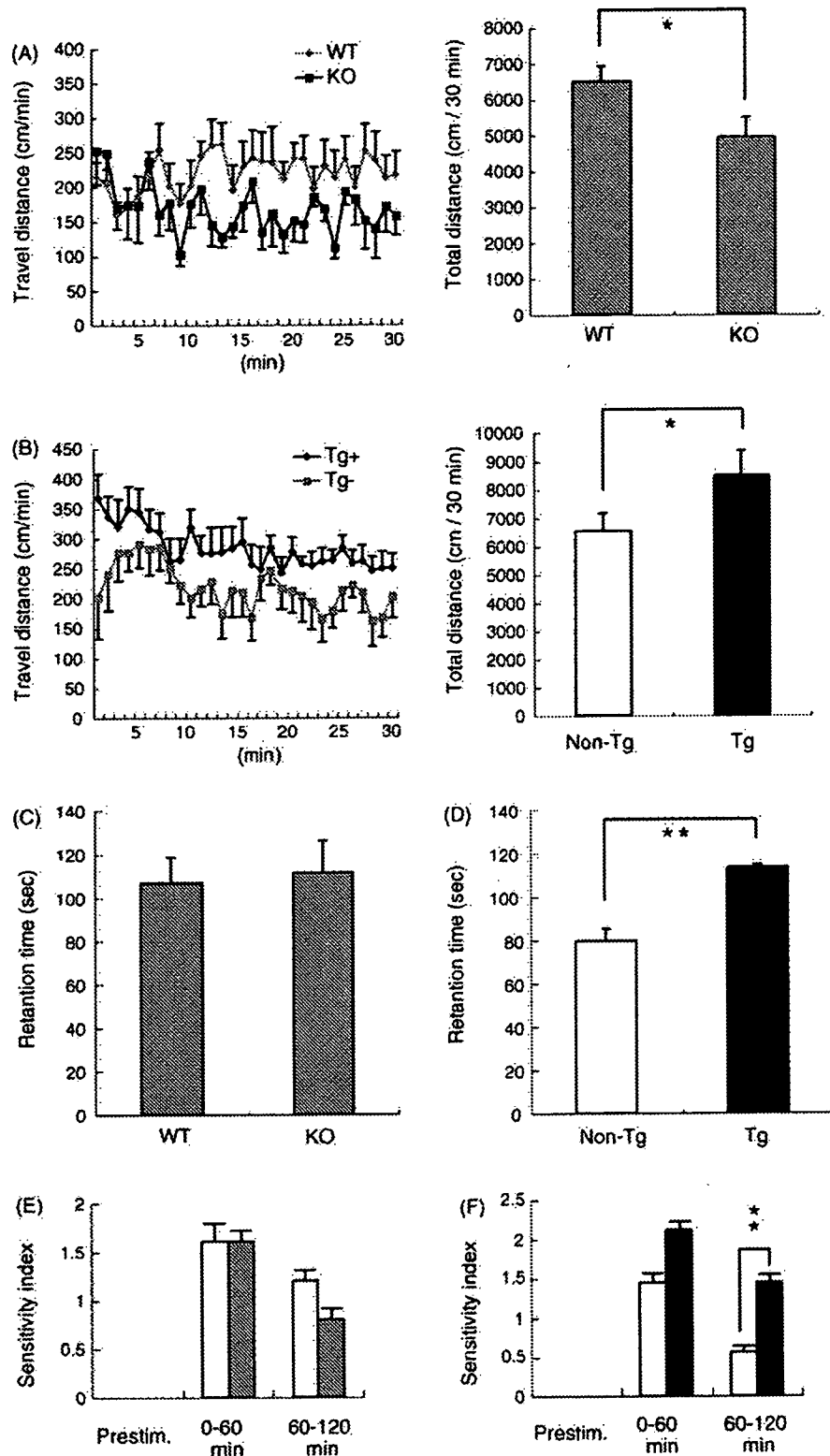
Fig. 4. Locomotor activity of Pael-R Tg and Pael-R KO mice. (A) Spontaneous horizontal migration of Pael-R KO ($n = 9$) and WT littermate ($n = 11$) mice at 1 year of age over a period of 30 min just after introduction into the open field chamber (50 cm × 50 cm). The migration distance in each minute interval after introduction (left) and total migration distance (right) are represented as mean ± S.E.M. (*$P < 0.05$ vs. WT; Student's t-test). (B) Spontaneous horizontal migration of PrP-Tg ($n = 11$) and non-Tg littermate ($n = 9$) mice at 1 year of age over a period of 30 min as in A. *$P < 0.05$ vs. non-Tg by Student's t-test. (C) Motor coordination of Pael-R KO and WT littermate mice at 1 year of age was assessed with the rotarod test ($n = 10$ each group). The retention time on a rotating wheel was consecutively measured four times. Each trial lasted for a maximum of 5 min, during which time the wheel rotates with a linear acceleration from 4 to 40 rpm. Data are represented as mean ± S.E.M. of retention time. (D) Motor coordination of PrP-Tg and non-Tg mice at 1 year of age was assessed with the rotarod test as in (C). (**$P < 0.01$ vs. non-Tg; Student's t-test, $n = 10$ each group). (E) The behavior of Pael-R KO and WT littermate male mice ($n = 5$ each group) during the free moving in vivo microdialysis analysis before and after METH administration (30 mg/kg) in Fig. 3A was scored as follows: 0, none; 1, piloerection without rotational motion; 2, slow rotational motion; 3, fast rotational motion or jumping movement. Mean ± S.E.M. of the score are represented as Sensitivity Index. Grey bars, KO mice; white bars, WT

3.2. Abnormal DA synthesis and metabolism by altered Pael-R expression

Pael-R Tg and KO mice are viable and present no gross anatomical abnormalities. Pael-R KO mice gained weight normally, whereas Pael-R Tg mice gained at a slower rate (37.1 ± 4.1 g in PrP-Tg *versus* 47.1 ± 2.1 g in PrP-non-Tg males at 10 months, $P < 0.05$, $n = 7$; 30.6 ± 1.9 g in PrP-Tg *versus* 38.5 ± 2.4 g in PrP-non-Tg females at 10 months, $P < 0.01$, $n = 14$; and 23.0 ± 1.7 g in PDGFβ-Tg *versus* 30.2 ± 1.8 g in PDGFβ-non-Tg males at 6 months, $P < 0.05$, $n = 9$).

Because Pael-R is abundantly expressed in the DA neurons and is implicated in the pathogenesis of PD, we then examined the effect of altered Pael-R expression on the nigrostriatal pathway. In the whole striatum tissue of Pael-R KO mice, DA, but not its precursor L-DOPA, levels were reduced to 60% of that in wild-type (WT) littermates (Fig. 2A). In contrast, striatal levels of DA were increased in both strains of Pael-R Tg mice (Fig. 2B and C). The levels of DOPAC were significantly increased only in PrP-Tg mice (Fig. 2B and C). In PrP-Tg mice, the concentration of extracellular DA (measured by *in vivo* microdialysis of freely moving mice) in the striatum as well as the concentration due to Ca^{2+}-dependent release at the presynapse of DA neurons was increased (Fig. 2D). The concentrations of extracellular DA and DOPAC (measured by *in vitro* microdialysis) were not significantly different in the striatum of Pael-R KO mice (data not shown).

3.3. Increased DA storage and release in Pael-R Tg mice

Administration of the psychostimulant methamphetamine (METH) stimulates DA release from the presynapse of DA neurons. METH administration (30 mg/kg, s.c.) induced a similar increase in extracellular DA levels in Pael-R KO and WT littermate mice (Fig. 3A). No increase occurred when 100 mM KCl was infused intrastriatally *via* a microdialysis probe at 270 min after METH, suggesting that 30 mg/kg METH is sufficient to the release of almost all DA stored in the presynapse. By contrast, METH administration (30 mg/kg, s.c.) stimulates a significant increase ($\sim$1.6-fold) in extracellular DA level in PrP-Tg compared with non-Tg mice ($P < 0.001$ by repeated measures ANOVA; Fig. 3B). Following METH administration, dialysate levels of DOPAC were decreased similarly in both PrP-Tg and PrP-non-Tg mice as well as Pael-R KO mice (data not shown), suggesting that METH inhibits monoamine oxidase activity as previously reported (Fumagalli et al., 1998). Although actual value of DA efflux was larger in male mice than in female mice, there was no sex difference in the ratio of peak DA levels to basal DA levels (Fig. 3C and D).

3.4. Behavioral phenotype by mice with altered Pael-R expression

DA content in the striatum plays an important role in the control of locomotor and stereotypic behavior. Changes in DA levels in these mice led us to test locomotor activity. The spontaneous locomotor activity of naïve Pael-R KO mice was significantly reduced in an initial 30-min trial (Fig. 4A). However, whereas the locomotor activity of Pael-R KO mice did not change every month, that of WT littermates gradually declined, probably because of habituation to the test. Consequently, locomotor activity was higher in Pael-R KO mice than WT littermates 5 months later (data not shown). The result suggests that Pael-R KO mice somewhat lose the ability of habituation to a circumstance. In contrast to Pael-R KO mice, both PrP-Tg and PDGFβ-Tg mice showed elevated locomotor activity in the same test (Fig. 4B and data not shown).

Motor performance was assessed by the rotarod test as described previously (Tateno et al., 2004). The rotarod scores measured of 6-month-old and 1-year-old Pael-R KO mice were not significantly changed whereas 1-year-old PrP-Tg showed the significant improvement in this test (Fig. 4C and D and data not shown). The phenotypes of Pael-R Tg mice in the locomotor test and the rotarod test might be suggested to reflect an elevated extracellular DA content.

Behavior in response to the METH-treatment (30 mg/kg, s.c.) was assessed in Pael-R KO mice and PrP-Tg mice (Fig. 4E and F). The responses to METH of Pael-R KO male mice did not significantly differ from that of their WT male littermates (Fig. 4E). However, these responses were more sensitive in PrP-Tg mice than in non-Tg littermates (Fig. 4F). These results correlated well with the DA release data obtained in the *in vivo* microdialysis experiment (Fig. 3A and B). The female responses tended to be milder than male, although levels of Pael-R protein expression in the brain were not different between male and female PrP-Tg mice (data not shown).

3.5. Sensitivity to DA neurotoxins

The numbers of TH-immunoreactive neurons in the SN, the ventral tegmental area (VTA) and the locus coeruleus of Pael-R KO and PrP-Tg mice (which are highly expressed in the locus coeruleus as well as the SN and VTA unlike PDGFβ-Tg mice) showed age-dependent loss of TH-positive neurons (manuscript in submission). The number of TH neurons in Pael-R KO mice showed a slight reduction compared with their WT littermates (Fig. 5A). However, the number did not change over time, suggesting that Pael-R somewhat contribute to developmental regulation of TH-positive neurons (data not shown).

Parkin KO mice have an increased extracellular DA and whole striatal DOPAC levels (Goldberg et al., 2003; Itier et al., 2003). Both Parkin KO mice and Pael-R Tg mice appear to have

littermates; Prestim., before METH-treatment; 0–60 min, for the first 1 h of METH-treatment; 60–120 min, for the second 1 h. (F) The behavior of PrP-Tg and non-Tg mice ($n = 5$ males; $n = 4$ females in each genotype) in METH administration (30 mg/kg) was scored as in (D). The score representing the sensitivity to METH is higher in the second 1 h after METH administration compared with non-Tg littermate (**$P < 0.01$ by Mann–Whitney U-test). Black bars, Tg mice; and white bars, non-Tg littermates.
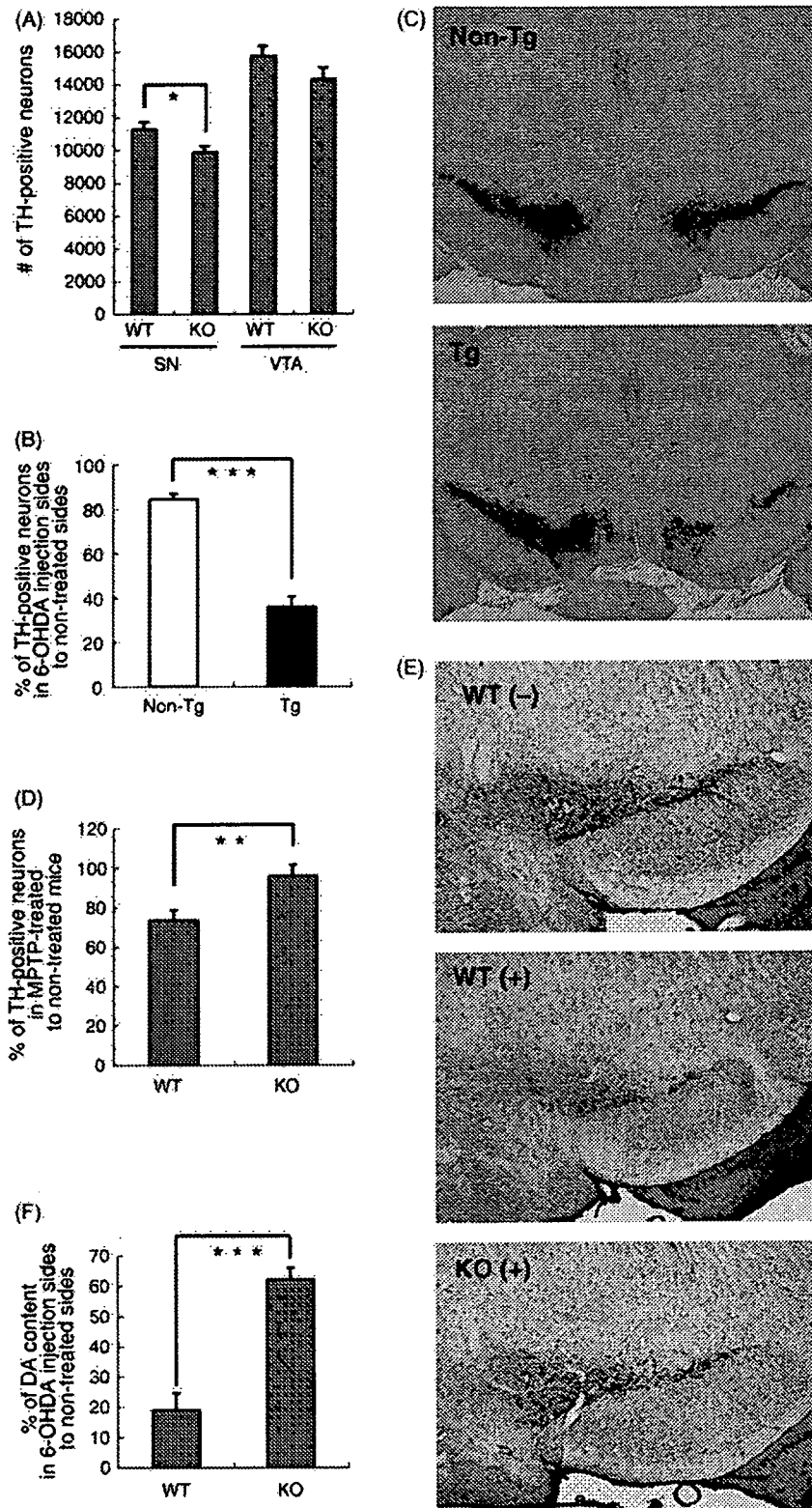
Fig. 5. Sensitivity of DA neurons to the neurotoxins in Pael-R Tg and Pael-R KO mice. (A) The estimated number of TH-positive neurons in the SN and VTA of Pael-R KO and WT littermate mice at 3 months of age was assessed by a stereological method (mean ± S.E.M., n = 7 mice). $*P < 0.05$ vs. WT littermates by Student's t-test. (B) Effect of 6-OHDA on DA neurons of Pael-R Tg mice 21 days after administration. 6-OHDA was injected into the left striatum of PrP-Tg and non-Tg littermate mice at 2–3 months of age. The number of TH-immunopositive neurons in the SN was assessed by a stereological method. To correct for genotype-based differences in the number of TH-positive cells, data are represented as percentage of the number on the non-treated side (right striatum) of each animal (mean ± S.E.M., Tg, n = 8; non-Tg, n = 9). $***P < 0.001$ vs. non-Tg by Student's t-test. (C) Representative coronal sections of 6-OHDA-treated non-Tg (upper) and Tg (lower) brains containing the SN are shown. The 6-OHDA-treated SN is located on the left side. (D) Effect of MPTP on DA neurons of Pael-R KO mice 7 days after administration. MPTP was injected into Pael-R KO and WT littermate mice at 3 months of age. Data are represented as percentage of the number of DA neurons in the SN in each pair with saline treatment (mean ± S.E.M., n = 8 per each group). $**P < 0.01$ vs. non-Tg by Student's t-test. (E) Representative coronal sections of